

**UCSF**

**UC San Francisco Electronic Theses and Dissertations**

**Title**

Dissection of the Neural Effects of Deep Brain Stimulation

**Permalink**

<https://escholarship.org/uc/item/4pd9p3dv>

**Author**

Schor, Jonathan Samuel

**Publication Date**

2020

Peer reviewed|Thesis/dissertation

Dissection of the Neural Effects of Deep Brain Stimulation

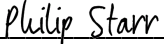
by  
Jonathan Schor

DISSERTATION  
Submitted in partial satisfaction of the requirements for degree of  
DOCTOR OF PHILOSOPHY

in  
Neuroscience

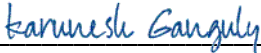
in the  
GRADUATE DIVISION  
of the  
UNIVERSITY OF CALIFORNIA, SAN FRANCISCO

Approved:

DocuSigned by:  
  
Philip Starr  
ADB44FC349C54C9...  
Chair

DocuSigned by:  
  
Alexandra Nelson

DocuSigned by:  
  
Joshua Berke

DocuSigned by:  
  
Karunesh Ganguly  
537133AC2605407...

---

Committee Members

Copyright 2020  
by  
Jonathan Schor

## Acknowledgements

The work in this thesis was done with the support of a Ruth Kirchstein F31 National Science Research Award Fellowship as well as a UCSF Discovery Fellowship.

I have always felt that, in order to work the long hours of science and face the inevitable ups and downs, it helps to be just a little obsessed with what you're doing. For the last four years, I've had the absolute pleasure of being surrounded by people who have helped to shape that obsession in a healthy way, sharing ideas, support, and mentorship, and who have also helped me to enjoy the world outside of science.

First, to my thesis advisor Alexandra Nelson, thank you for being the exemplar of a physician-scientist that I will always use to guide me. You're a tremendous mentor, an incredible thinker, and a compassionate and wonderful friend. None of the work detailed in this thesis would have been possible without Alexandra's insight and keen mind, nor would I have accomplished nearly as much without her support and encouragement.

To the members of the Nelson lab, because of all of you these last four years have been more fun and enriching than I could have ever imagined. Particularly to Ally, Mike, and Match, you three have essentially been members of my family while living in San Francisco. You've always been there for me both in lab and out, and I can't wait to continue to see you all as we progress through our scientific careers.

Thank you also to my thesis committee, Phillip Starr, Josh Berke, and Karunesh Ganguly, who have all been instrumental in shaping both the project detailed here and my future career path.

Thank you to the administrators of the MSTP and Neuroscience programs, Geri Ehle, Pat Veitch, and Lucita Nacionales. You've helped to guide me through this whole process, even at my most clueless, with patience and compassion.

Additionally, thank you also to all of my friends for your support and encouragement throughout this process, and for reminding me that there's always time to go on another adventure.

Finally, thank you to my family. To my parents, Nina and Robert, listening to your excited conversations at the dinner table showed me just how much fun a career in science could be. To my brothers, Stanford and Asher, both of you are the funniest, coolest, and smartest people I know, and I'm so glad that we've all been able to live in the Bay together these past few years. And to my wife, Stephany: You're the most amazing partner I could imagine, thank you for all of your love and support. I'm so glad we're on this crazy ride together.

# Dissection of the Neural Effects of Deep Brain Stimulation

Jonathan Schor

## **Abstract**

Deep brain stimulation (DBS) is a clinical and investigational treatment for a variety of neuropsychiatric conditions, such as Parkinson's Disease (PD) and obsessive-compulsive disorder. Despite widespread clinical use, its therapeutic mechanism is unknown. Previous results indicate DBS may produce a complex array of effects, ranging from inhibition in the STN to antidromic stimulation of cortical afferents, but it has proven difficult to establish how these changes interact to alter behavior. Here, we developed a mouse model of subthalamic nucleus (STN) DBS for PD to investigate this question using the mechanistic and cell type-specific tools available in mice.

First, in Chapter 1 (Introduction) I detail various theories surrounding the mechanism of STN DBS and discuss the technical limitations that have prevented a definitive exploration from taking place.

In Chapter 2 (Multiple stimulation parameters influence efficacy of deep brain stimulation in parkinsonian mice), I describe the development of a mouse model of electrical STN DBS for PD, and demonstrate that it recapitulates many of the salient features of STN DBS in human PD patients. I also describe a composite metric which can be used to characterize the relationship of DBS parameters to their behavioral efficacy in mice, and show that this relationship holds when the metric was applied retrospectively to human data.

In Chapter 3 (Levodopa and STN Deep Brain Stimulation Relieve Parkinsonian Motor Symptoms with Opposing Changes in Basal Ganglia Activity), I report our findings using optical tools in a mouse model of PD, recording calcium signals as a surrogate marker of neural activity. In concordance with previous electrophysiological studies, we find that in parkinsonian mice, dopamine replacement therapy with levodopa causes large *decreases* in neural activity at the level of basal ganglia output (the substantia nigra pars reticulata, or SNr). In contrast, therapeutic electrical STN DBS *increases* activity in both the STN and SNr. Furthermore, we find that both optogenetic inhibition of SNr neurons, which mimics the effects of levodopa, and optogenetic excitation of STN neurons, which mimics the effects of STN DBS, are therapeutic in mice.

Finally, in Chapter 4 (Conclusions), we discuss the implications of these findings and the role of future studies in further elucidating the mechanism of STN DBS.

# Table of Contents

<b>Chapter 1: Introduction.....</b>	<b>1</b>
<b>Chapter 2: Multiple stimulation parameters influence efficacy of deep brain stimulation in parkinsonian mice .....</b>	<b>11</b>
Abstract .....	12
Introduction .....	13
Results .....	14
Discussion .....	21
Methods .....	22
<b>Chapter 3: Levodopa and STN Deep Brain Stimulation Relieve Parkinsonian Motor Symptoms with Opposing Changes in Basal Ganglia Activity.....</b>	<b>49</b>
Abstract .....	50
Introduction .....	51
Results .....	53
Discussion .....	61
Methods .....	66
<b>Chapter 4: Conclusion .....</b>	<b>94</b>



# List of Figures

## Chapter 1

Figure 1.1. Model of the basal ganglia in health and disease. .... 10

## Chapter 2

Figure 2.1. Subthalamic nucleus deep brain stimulation (STN DBS) alleviates bradykinesia in parkinsonian mice across a wide range of frequencies. .... 34

Figure 2.2. STN DBS in parkinsonian mice recapitulates key features of human DBS. .... 35

Figure 2.3. Effectiveness of STN DBS depends linearly on a composite stimulation parameter metric,  $p^{\text{combo}}$ . .... 36

Supplemental Figure 2.1. STN DBS improves multiple movement metrics in hemiparkinsonian mice. .... 38

Supplemental Figure 2.2. Both dyskinesia and DBS efficacy scale with  $p_i^{\text{combo}}$ . .... 39

Supplemental Figure 2.3. Modeling DBS using  $p_i^{\text{combo}}$  predicts the therapeutic parameter space. .... 41

Supplemental Figure 2.4. Movement velocity and dyskinesia relationships to  $p_i^{\text{combo}}$  by stimulation sites across individual mice..... 42

## Chapter 3

Figure 3.1. Deep brain stimulation (DBS) of the subthalamic nucleus (STN) increases STN activity..... 81

Figure 3.2. STN DBS and levodopa have opposite effects on activity in the substantia nigra pars reticulata (SNr). .....	82
Figure 3.3. The responses of hyperdirect primary motor cortex (M1) neurons to STN DBS do not consistently correlate with motor benefits. ....	85
Figure 3.4. Optogenetic inhibition of SNr and optogenetic excitation of STN increase movement in parkinsonian mice. ....	86
Supplemental Figure 3.1. Related to Figure 3.1. Levodopa and STN DBS produce similar behaviors in parkinsonian mice. ....	88
Supplemental Figure 3.2. Related to Figure 3.1. STN stimulation increases STN activity in vitro and in vivo. ....	89
Supplemental Figure 3.3. Related to Figure 3.2. STN DBS evokes a rapid increase in SNr activity. ....	91
Supplemental Figure 3.4. Related to Figure 3.3. STN DBS drives inconsistent and slow changes to hyperdirect M1 activity. ....	92
Supplemental Figure 3.5. Related to Figure 3.4. The time course of optically evoked changes in ex vivo firing rate parallel those in in vivo movement velocity. ....	93

## List of Tables

### Chapter 2

Supplemental Table 2.1. Early DBS Parameters. ....	43
Supplemental Table 2.2. Late DBS Parameters. ....	45
Supplemental Table 2.3. Human DBS Parameters.....	48

# **Chapter 1:**

## **Introduction**

## Introduction

The basal ganglia are a group of interconnected subcortical nuclei critical for movement, action selection, and motor learning<sup>1</sup>. These nuclei have also been implicated in a variety of neurological disorders, including Huntington's Disease, dystonia, and Parkinson's Disease (PD)<sup>2</sup>. In PD, the progressive loss of midbrain dopamine neurons and their projections to the input nucleus of the basal ganglia, the striatum, is believed to result in altered signaling in striatal direct and indirect pathway medium spiny neurons (dMSNs and iMSNs, respectively)<sup>2-4</sup> (Fig 1.1 left and middle). According to the standard, or rate model of basal ganglia function, decreased dopamine produces overactivity in the indirect pathway, leading to decreases in the amplitude and velocity of voluntary movement<sup>3</sup>. Many PD motor symptoms are thus hypothesized to arise from abnormalities in neural activity.

There are no disease-modifying therapies available for PD, but there are two major classes of symptomatic treatment, both of which focus on the motor symptoms: (1) dopamine replacement therapy and (2) Deep Brain Stimulation (DBS). The dopamine precursor levodopa boosts dopamine levels in the brain, and is hypothesized to restore a balance in the activity of the direct and indirect pathways, leading to improved motor function. Levodopa indeed alleviates many PD motor symptoms<sup>5</sup>. With chronic treatment, however, patients often develop motor fluctuations, including unpredictable benefits with each dose of levodopa, and drug-induced dyskinesias. If such fluctuations cannot be adequately managed with changes in dosing, many patients seek basal ganglia DBS. Electrical stimulation devices are most commonly implanted in the STN, a downstream target of the indirect pathway<sup>6</sup> (Fig 1.1, right), though the globus pallidus pars interna

(GPi) is another common target. Basal ganglia DBS alleviates many of the motor symptoms of PD, allowing patients to drastically reduce their reliance on dopaminergic agents, thereby improving motor fluctuations. Despite the use of STN DBS for several decades, its mechanism of action remains unknown.

STN electrical stimulation may cause changes in the activity of (1) local STN cell bodies and their axons, (2) inputs to the STN from a variety of other structures, or (3) axons of passage. Which of these potential changes mediate the therapeutic effects of DBS is unknown. Initially, it was postulated that STN DBS relieved parkinsonian symptoms by inhibiting STN neurons and the nuclei to which they project, a theory based on the observation that in parkinsonian non-human primates (NHPs), STN lesions resulted in marked motor improvements<sup>7</sup>. Indeed, in humans, subthalamotomy also relieves parkinsonism<sup>8</sup>. According to this model, reducing STN activity would lead to decreased basal ganglia output, facilitating movement<sup>2,3</sup> (Fig 1.1, right). Supporting this idea, some *in vitro* electrophysiological evidence has suggested that high frequency stimulation (HFS) may drive STN neurons into depolarization block, preventing further action potential firing<sup>9</sup>. Some *in vivo* electrophysiological studies also suggest STN cell bodies may be inhibited during HFS DBS<sup>10,11</sup>. However, these latter results are challenging to interpret, due stimulation artifacts in electrical recordings. Typical STN DBS requires continuous electrical stimulation at 120-180 Hz, which obscures the 20-40 Hz firing rates of STN neurons during electrophysiological recordings; even attempts at removing these artifacts may unintentionally alter the underlying data. In humans, direct recordings of the output nuclei can rarely be made during STN DBS<sup>12</sup>, and likewise few such recordings exist in animal models (NHPs<sup>13</sup> or rats<sup>14</sup>). In addition, the heterogeneity

of cell types in basal ganglia nuclei make it possible that changes in one population of neurons might be hidden by opposing changes in other populations<sup>15</sup>, a phenomenon that could be detected using cell type-specific genetic tools now available in mice.

In an effort to better understand how DBS relieves parkinsonian symptoms, previous rodent studies have used optogenetics to mimic STN DBS with pulsed light<sup>16,17</sup>. These studies have led to a competing theory involving the hyperdirect pathway, which carries excitatory projections from the cortex to the STN<sup>18,19</sup> (Fig 1.1, orange). According to this theory, electrical STN DBS causes antidromic activation of a population of cortical neurons that project to the STN. A systematic dissection of the afferent circuitry to the STN using optogenetics in mice revealed that high frequency activation of STN-projecting primary motor cortex (M1) neurons (hyperdirect pathway) was sufficient to recapitulate many of the therapeutic benefits seen in STN DBS patients<sup>16,17</sup>. While it is unclear how well optical stimulation mirrors electrical DBS as used in human patients, subsequent research showed that in a rat model, as well as in patients, electrical STN DBS indeed does evoke antidromic spikes in M1 afferents and disrupts cortical rhythmic oscillations seen during parkinsonism<sup>20–22</sup>. These results are consistent with, but do not prove, the idea that antidromic stimulation of cortical inputs underlies the therapeutic effects of electrical STN DBS. Unfortunately, while these studies generated several theories of how DBS works<sup>23</sup>, their technical limitations and distinct differences from DBS as used in PD patients (electrical artifacts, optical rather than electrical stimulation) prevent directly testing whether hyperdirect pathway mechanisms are required for the therapeutic effects of STN DBS.

Though initial theories about how DBS altered neural circuits and produced therapeutic effects in PD focused on changes in firing *rate*, accumulating data in human patients as well as animal models suggest that the pathophysiology of PD might more closely relate to changes in firing pattern at the individual or ensemble level. Multiple groups have found changes in the bursting of basal ganglia neurons<sup>12,13,24</sup>, as well as alterations in the local field potential (LFP) in PD and in animal models<sup>25</sup>. Since these discoveries, investigators have also found that beta oscillations correlate with disease symptoms<sup>26</sup>, and are reduced in response to treatment with either levodopa<sup>27</sup> or STN DBS<sup>28</sup>. Over the past two decades, theories regarding therapeutic mechanisms of STN DBS have increasingly revolved around the idea that pathological oscillations are disrupted by therapeutic manipulations.

Though STN DBS broadly impacts neural circuitry, it is unknown which changes are critical to its therapeutic benefit. Perhaps the most critical roadblock is the inability to perform electrical STN DBS while using cell type-specific techniques to monitor and manipulate neural activity in the STN and connected nuclei. Fortunately, when I began my inquiry a number of methods became available that allow for optical recordings in freely moving mice, with the caveat that no one had previously characterized the effect of STN DBS in a parkinsonian mouse model. Therefore, through a combination of electrode engineering and stereotactic targeting, we developed a mouse model of STN DBS in PD and used it to address some of the key questions in the field:

- (1) What is the parameter space for therapeutic STN DBS?
- (2) What is the effect of STN DBS on STN and SNr activity *in vivo*?
- (3) Which of the changes caused by STN DBS produce therapeutic benefit?



## References

1. Turner, R. S. & Desmurget, M. Basal Ganglia Contributions to Motor Control: A Vigorous Tutor. *Curr. Opin. Neurobiol.* **20**, 704–716 (2010).
2. DeLong, M. R. Primate models of movement disorders of basal ganglia origin. *Trends Neurosci.* **13**, 281–285 (1990).
3. Albin, R. L., Young, A. B. & Penney, J. B. The functional anatomy of basal ganglia disorders. *Trends Neurosci.* **12**, 366–375 (1989).
4. Gerfen, C. R. *et al.* D1 and D2 dopamine receptor-regulated gene expression of striatonigral and striatopallidal neurons. *Science* **250**, 1429–1432 (1990).
5. Ovalath, S. & Sulthana, B. Levodopa: History and Therapeutic Applications. *Ann. Indian Acad. Neurol.* **20**, 185–189 (2017).
6. Obeso, J. A. *et al.* Surgical treatment of Parkinson's disease. *Baillieres Clin. Neurol.* **6**, 125–145 (1997).
7. Bergman, H., Wichmann, T. & DeLong, M. R. Reversal of experimental parkinsonism by lesions of the subthalamic nucleus. *Science* **249**, 1436–1438 (1990).
8. Su, P. C., Tseng, H.-M., Liu, H.-M., Yen, R.-F. & Liou, H.-H. Subthalamotomy for advanced Parkinson disease. *J. Neurosurg.* **97**, 598–606 (2002).
9. Do, M. T. H. & Bean, B. P. Subthreshold Sodium Currents and Pacemaking of Subthalamic Neurons: Modulation by Slow Inactivation. *Neuron* **39**, 109–120 (2003).

10. Filali, M., Hutchison, W. D., Palter, V. N., Lozano, A. M. & Dostrovsky, J. O. Stimulation-induced inhibition of neuronal firing in human subthalamic nucleus. *Exp. Brain Res.* **156**, 274–281 (2004).
11. Moran, A., Stein, E., Tischler, H., Bebelovsky, K. & Bar-Gad, I. Dynamic Stereotypic Responses of Basal Ganglia Neurons to Subthalamic Nucleus High-Frequency Stimulation in the Parkinsonian Primate. *Front. Syst. Neurosci.* **5**, (2011).
12. Reese, R. *et al.* Subthalamic deep brain stimulation increases pallidal firing rate and regularity. *Exp. Neurol.* **229**, 517–521 (2011).
13. Hashimoto, T., Elder, C. M., Okun, M. S., Patrick, S. K. & Vitek, J. L. Stimulation of the subthalamic nucleus changes the firing pattern of pallidal neurons. *J. Neurosci.* **23**, 1916–1923 (2003).
14. Shi, L.-H., Luo, F., Woodward, D. J. & Chang, J.-Y. Basal ganglia neural responses during behaviorally effective deep brain stimulation of the subthalamic nucleus in rats performing a treadmill locomotion test. *Synapse* **59**, 445–457 (2006).
15. Rommelfanger, K. S. & Wichmann, T. Extrastriatal Dopaminergic Circuits of the Basal Ganglia. *Front. Neuroanat.* **4**, (2010).
16. Gradinaru, V., Mogri, M., Thompson, K. R., Henderson, J. M. & Deisseroth, K. Optical Deconstruction of Parkinsonian Neural Circuitry. *Science* **324**, 354–359 (2009).

17. Sanders, T. H. & Jaeger, D. Optogenetic stimulation of cortico-subthalamic projections is sufficient to ameliorate bradykinesia in 6-ohda lesioned mice. *Neurobiol. Dis.* **95**, 225–237 (2016).
18. Nambu, A., Takada, M., Inase, M. & Tokuno, H. Dual somatotopical representations in the primate subthalamic nucleus: evidence for ordered but reversed body-map transformations from the primary motor cortex and the supplementary motor area. *J. Neurosci.* **16**, 2671–2683 (1996).
19. Nambu, A., Tokuno, H. & Takada, M. Functional significance of the cortico–subthalamo–pallidal ‘hyperdirect’ pathway. *Neurosci. Res.* **43**, 111–117 (2002).
20. Li, Q. *et al.* Therapeutic Deep Brain Stimulation in Parkinsonian Rats Directly Influences Motor Cortex. *Neuron* **76**, 1030–1041 (2012).
21. de Hemptinne, C. *et al.* Therapeutic deep brain stimulation reduces cortical phase-amplitude coupling in Parkinson’s disease. *Nat. Neurosci.* **18**, 779–786 (2015).
22. Miocinovic, S. *et al.* Cortical potentials evoked by subthalamic stimulation demonstrate a short latency hyperdirect pathway in humans. *J. Neurosci.* 1327–18 (2018)  
doi:10.1523/JNEUROSCI.1327-18.2018.
23. Chiken, S. & Nambu, A. Disrupting neuronal transmission: mechanism of DBS? *Front. Syst. Neurosci.* **8**, (2014).

24. Pan, M.-K. *et al.* Neuronal firing patterns outweigh circuitry oscillations in parkinsonian motor control. *J. Clin. Invest.* **126**, 4516–4526 (2016).
25. Stein, E. & Bar-Gad, I. Beta oscillations in the cortico-basal ganglia loop during parkinsonism. *Exp. Neurol.* **245**, 52–59 (2013).
26. Little, S. & Brown, P. The functional role of beta oscillations in Parkinson’s disease. *Parkinsonism Relat. Disord.* **20 Suppl 1**, S44-48 (2014).
27. Halje, P. *et al.* Levodopa-Induced Dyskinesia Is Strongly Associated with Resonant Cortical Oscillations. *J. Neurosci.* **32**, 16541–16551 (2012).
28. Little, S. *et al.* Adaptive Deep Brain Stimulation In Advanced Parkinson Disease. *Ann. Neurol.* **74**, 449–457 (2013).

**Figure 1.1**

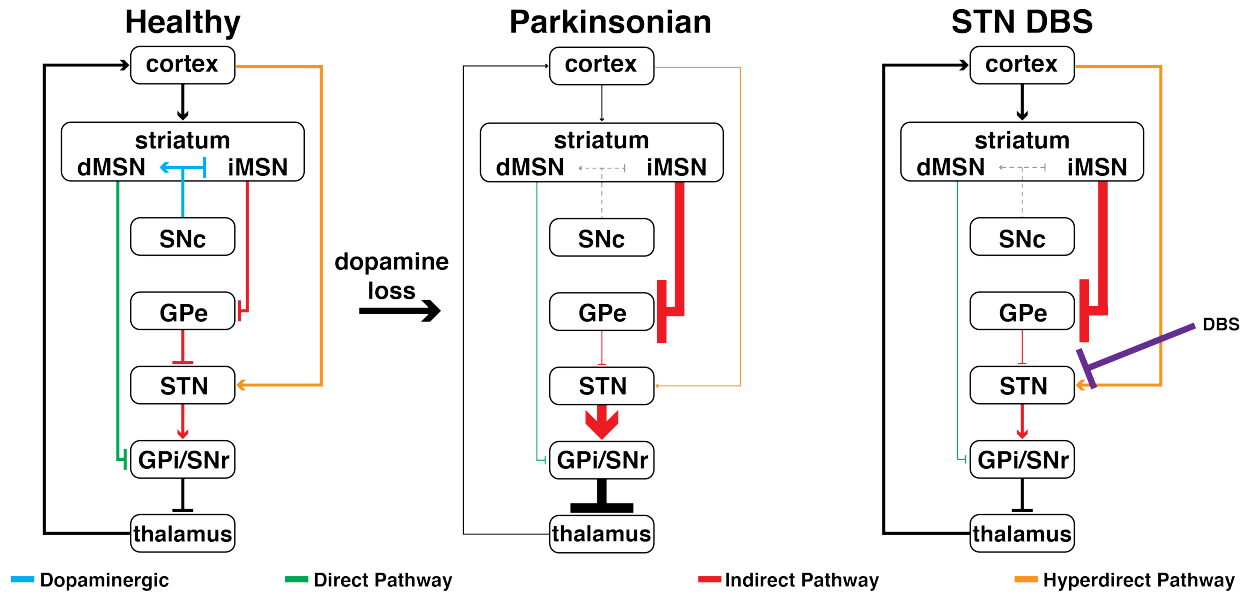


**Figure 1.1. Model of the basal ganglia in health and disease.** A schematic depicting the classical rate model of the basal ganglia in both a healthy mouse and a parkinsonian mouse following dopamine depletion, as well as one of the proposed mechanisms for STN DBS ( $\downarrow$  = excitatory,  $\perp$  = inhibitory).

## Chapter 2:

# Multiple stimulation parameters influence efficacy of deep brain stimulation in parkinsonian mice<sup>‡</sup>

<sup>‡</sup>A version of this chapter was published as Schor JS, Nelson AB. Multiple stimulation parameters influence efficacy of deep brain stimulation in parkinsonian mice. *The Journal of Clinical Investigation*. 2019 June 13;130:3833-3838.

# **Multiple stimulation parameters influence efficacy of deep brain stimulation in parkinsonian mice**

## **Abstract**

Deep brain stimulation (DBS) is used to treat multiple neuropsychiatric disorders, including Parkinson's Disease (PD). Despite widespread clinical use, its therapeutic mechanisms are unknown. Here, we developed a mouse model of subthalamic nucleus (STN) DBS for PD, to permit investigation using cell type-specific tools available in mice. We found that electrical STN DBS relieved bradykinesia, as measured by movement velocity. In addition, our model recapitulated several hallmarks of human STN DBS, including rapid onset and offset, frequency dependence, dyskinesia at higher stimulation intensity, and associations between electrode location, therapeutic benefit, and side effects. We used this model to assess whether high frequency stimulation is necessary for effective STN DBS, or if low frequency stimulation can be effective when paired with compensatory adjustments in other parameters. We found that low frequency stimulation, paired with greater pulse width and amplitude, relieved bradykinesia. Moreover, a composite metric incorporating pulse width, amplitude, and frequency predicted therapeutic efficacy better than frequency alone. We found a similar relationship between this composite metric and movement speed in a retrospective analysis of human data, suggesting correlations observed in the mouse model may extend to human patients. Together, these data establish a mouse model for elucidating mechanisms of DBS.

## Introduction

Parkinson's Disease (PD) is a neurodegenerative disease characterized by motor deficits, including bradykinesia (slowed movement), rigidity, and tremor. Dopamine replacement therapy relieves many motor symptoms, but is often complicated by the development of prominent motor fluctuations and involuntary movements<sup>1</sup>. With few effective pharmacological alternatives, patients are often implanted with electrodes in basal ganglia nuclei for chronic stimulation. Deep brain stimulation of the subthalamic nucleus (STN DBS)<sup>2</sup> is highly effective in relieving bradykinesia, rigidity, and tremor<sup>3</sup>. Despite several decades of clinical experience, however, the underlying mechanisms and ideal therapeutic parameters for STN DBS remain unclear<sup>4</sup>.

The basal ganglia circuit in PD patients exhibits abnormal firing rate, pattern, and synchronization<sup>5</sup>; STN DBS may disrupt or correct one or a number of these changes. At present, clinical practice is delivery of continuous pulsatile stimulation at high frequency. Therapeutic benefit depends on the frequency, current amplitude, and pulse width of stimulation<sup>4</sup>. One theory postulates that high frequency stimulation (HFS, over 90Hz) disrupts abnormal basal ganglia activity<sup>6</sup>, while other parameters (pulse width and current) may allow spread of stimulation through the STN. In fact, HFS provides greater relief of bradykinesia and tremor, whereas very low frequency stimulation (LFS, around 10Hz) can be ineffective or even potentially deleterious<sup>7</sup>. However, a less widely held hypothesis is that any manipulation that perturbs neuronal firing may disrupt abnormal activity, and thus clinicians can compensate for a low setting of any one parameter (frequency, pulse width, or current) by increasing the other two; one study found the current amplitude necessary to relieve rigidity varied inversely with the pulse width<sup>8</sup>. A



better understanding of how individual parameters contribute to STN DBS efficacy would not only improve symptom management in patients, but might also identify potential therapeutic mechanisms of STN DBS.

Though electrical DBS has been demonstrated in both parkinsonian nonhuman primates<sup>9,10</sup> and rats<sup>11,12</sup>, a mouse model, combined with the extensive mouse genetic toolbox, would permit complementary cellular and circuit investigations of DBS therapeutic mechanisms. Here, we developed a mouse model of STN DBS in hemiparkinsonian mice. Stimulation relieves bradykinesia and recapitulates a number of features of STN DBS in human patients. We use this model to investigate the relationship between stimulation parameters and therapeutic efficacy, as well as adverse effects, and find that a composite metric based on all three stimulation parameters predicts STN DBS efficacy. This relationship also holds in a retrospective analysis of human data, suggesting shared therapeutic features in human and mouse STN DBS. Together, our results provide a valuable tool for predicting DBS efficacy, as well as a model for further investigation of STN DBS.

## **Results**

Parkinsonian mouse models have contributed to our understanding of both disease pathophysiology and the actions of levodopa<sup>5</sup>. However, it is not known whether parkinsonian mice respond to electrical STN DBS in similar ways to patients. We identified six clinical features of STN DBS for PD, which we used as criteria in a mouse model of STN DBS: (1) STN DBS reduces bradykinesia, (2) motor benefits are time-locked to stimulation, (3) relief of bradykinesia is frequency dependent<sup>13</sup>; (4) increasing stimulation intensity (across multiple parameters) results in dyskinesia<sup>14</sup>; (5) dorsal STN

stimulation is more effective than ventral stimulation in relieving bradykinesia<sup>15</sup>; (6) and stimulation closer to the pyramidal tract is more likely to evoke motor contractions<sup>16</sup>.

With these criteria in mind, we designed and implanted unilateral 6-lead electrodes (divided into 3 bipolar pairs) in the STN of adult hemiparkinsonian mice, using the unilateral 6-hydroxydopamine (6-OHDA) model (Figure 2.1A-C). In these mice, parkinsonism was manifest as both ipsilesional rotational bias (Supplemental Figure 2.1G, see pre vs healthy) and decreased movement velocity (Figure 2.1H, see pre vs healthy). We used the latter indicator as a measure of bradykinesia, though it may also incorporate other parkinsonian features such as gait dysfunction. We constructed our 6-lead electrodes to span ~300-600 $\mu$ m (covering the ~250 $\mu$ m vertical span of mouse STN) and implanted them in the ipsilesional STN (Figure 2.1D-E, Supplemental Figure 2.1A-B). We selected the optimal electrode pair by stimulating at settings mirroring typical human DBS and DBS in rat models<sup>12,17</sup> (120Hz, 200 $\mu$ A, 60 $\mu$ s with bipolar, biphasic square waves, Supplemental Figure 2.1C). The stimulated pair eliciting the highest average movement velocity was used for subsequent experiments (Supplemental Figure 2.1D). Stimulation at these DBS parameters increased movement velocity in mice (Figure 2.1F-G, Supplemental Video 1); velocity changed at short latency from onset (3.19 +/- 0.65 sec) and offset (0.66 +/- 0.10 sec) of stimulation, corroborating clinical features (1) and (2). We used 1-minute stimulation epochs to efficiently evaluate a wide array of stimulation parameter combinations but found that longer periods of stimulation (10 minutes) produced similar improvements in movement velocity (Supplemental Figure 2.1E). These findings suggest that STN DBS in parkinsonian mice and PD patients share core therapeutic features.

We next explored whether STN DBS in hemiparkinsonian mice shows frequency dependence, as has been observed in humans (criterion 3)<sup>7,13</sup>. To address this question, we varied stimulation frequency while holding current amplitude and pulse width constant (200 $\mu$ A and 60 $\mu$ s). Movement velocity scaled relatively linearly with frequency up to approximately 120Hz (Figure 2.1H), mirroring observations in patients using hand tapping speed as the outcome measure<sup>13</sup>. However, the range of effective frequencies was much wider (as low as 15Hz) than reported in patients. In addition to absolute velocity, STN DBS also improved other well-established metrics<sup>17</sup> such as percent-time moving and relative velocity (normalized to pre-stim period) in a frequency-dependent manner, though rotational bias was not significantly changed (Supplemental Figure 2.1F-H). In humans, dyskinesia emerges as a side effect of higher frequency stimulation<sup>14</sup>. Likewise, we found that in mice, higher frequency stimulation, as well as increased pulse width and current, evoked dyskinesia<sup>18</sup> (Figure 2.2A). These findings suggest that in parkinsonian mice, as in humans, both therapeutic and dyskinetic effects of stimulation relate to stimulation frequency.

To assess the relationship of stimulation location to therapeutic efficacy and dyskinesia (criteria 5 and 6), we determined the location of DBS in postmortem tissue. Following terminal anesthesia, we made electrolytic lesions using the therapeutic leads (Figures 2.1E, 2.2B). We correlated dorso-ventral location with the relative velocity of each mouse at standard stimulation settings (120Hz, 200 $\mu$ A, and 60 $\mu$ s). As in humans, greater improvements in velocity were seen with more dorsal STN stimulation (Figure 2.2C). This may relate to targeting sensorimotor STN territories<sup>19,20</sup> or the zona incerta, stimulation of which is also therapeutic<sup>21,22</sup>. We next correlated electrode distance from

the pyramidal tract with the dyskinesia score in response to stimulation at 120Hz, 300 $\mu$ A, and 120 $\mu$ s (parameters which reliably evoked dyskinesias in over half of mice). Again, the mouse model mirrored human data: mice with electrodes closer to the pyramidal tract had greater dyskinesia (Figure 2.2D). Our model fulfilled all six clinical criteria, recapitulating key features of human DBS and indicating it may be a useful tool in understanding STN DBS mechanisms.

A dominant theory is that high- and low-frequency stimulation (HFS and LFS, respectively) produce qualitatively different changes in basal ganglia activity, and thus only HFS is efficacious<sup>7</sup>. Alternatively, any combination of frequency, current, and pulse width that sufficiently disrupts STN-basal ganglia circuit activity may be therapeutic. To test these theories using our model, we first assessed the relationship of each of the three variables (current, frequency, and pulse width) to movement velocity, while holding the other two constant. As we previously observed, movement velocity showed a strong linear correlation with frequency, when pulse width and current were held at constant (Figure 2.3A). However, we also observed strong linear relationships when only varying pulse width (Figure 2.3B) or current (Figure 2.3C), suggesting each variable individually contains linear predictive value. These individual parameters can also be combined in a metric cited in the clinical DBS literature: Total Electrical Energy Delivered (TEED)<sup>23</sup>. TEED is calculated as  $[current^2 * frequency * pulse\ width] / impedance$ . We found that current-squared, one term in this metric, was also linearly correlated with movement velocity (Figure 2.3D). Together, these results support the idea that many parameter combinations can provide therapeutic benefit.

While within the limited range tested, all three parameters correlated with therapeutic benefit, we wondered whether a combined metric might predict benefit across a wider set of parameters. If so, such a metric might prove a useful tool for clinicians. To explore this possibility, we stimulated using 31 different parameter combinations (Supplemental Figure 2.2A, Supplemental Table 2.1) and measured the resulting movement velocity. We collapsed each parameter combination into a single value ( $p_i^{\text{combo}}$ , where the “i” subscript indicates constant-current stimulation), calculated as *current*<sup>2</sup> \* *frequency* \* *pulse width*.  $p_i^{\text{combo}}$  is based on TEED, but we ascribe no physical meaning to this composite metric and use it only to compare different parameter combinations. We found that the effectiveness of DBS, as measured by movement velocity, scaled linearly with  $p_i^{\text{combo}}$  (Figure 2.3E). This relationship held across stimulation bouts when parameter combinations were grouped into three  $p_i^{\text{combo}}$  levels (Supplemental Figure 2.2B). These results also indicate many different parameter combinations may be effective.

In PD patients, optimal stimulation parameters often change over the first few months of DBS use; typically one or more parameters must be increased to maintain efficacy<sup>24</sup>, possibly related to alterations in both the electrodes and the surrounding tissue<sup>25</sup>. To test for this phenomenon in mice, we performed STN DBS in the same 9 mice at 50 new parameter combinations approximately two months later (Supplemental Figure 2.2A, Supplemental Table 2.2). Consistent with human data, mice showed less benefit from stimulation at later time points (Supplemental Figure 2.2C, comparing slopes of solid and dotted lines), but DBS efficacy again scaled linearly with  $p_i^{\text{combo}}$  (Supplemental Figure 2.2C). With these parameters we also manually scored dyskinesia and found severity scaled linearly with  $p_i^{\text{combo}}$  (Supplemental Figure 2.2D). These findings are consistent with

the idea that a composite metric incorporating stimulation pulse width, amplitude, and frequency consistently explains much of the variance in both the therapeutic and dyskinetic effects of STN DBS.

We next generated a model for DBS efficacy, using the regression between stimulation parameters and movement velocity in early DBS testing. This model was based on  $p_i^{\text{combo}}$  (Supplemental Figure 2.3A-D) and predicts that when current and pulse width are held at levels mimicking standard human stimulation, DBS efficacy will show frequency dependence (Supplemental Figure 2.3B-C). However, a more comprehensive exploration of parameter space revealed that increased pulse width and current amplitude can be used to compensate for reduced frequency, extending the range of effective DBS parameters. Similar results were observed when a model was created based on the regression from late DBS testing (Supplemental Figure 2.3E-H), though due to the shallower slope of the late DBS regression, the same combination of any three parameters produced less therapeutic benefit than in the early model. These models not only explain previous clinical observations but may provide valuable individualized visualizations of effective parameters for future PD patients.

To determine whether the  $p_i^{\text{combo}}$  metric could be used with individual stimulation site data to predict relationships between stimulation site and therapeutic efficacy and/or dyskinesia, we calculated a new metric for therapeutic efficacy. We calculated the slope of the correlation between  $p_i^{\text{combo}}$  and movement velocity (vel slope; Supplemental Figure 2.4A), representing the additional benefit derived from unit increases in  $p_i^{\text{combo}}$ . We found that electrode location along the dorso-ventral axis showed a modest correlation with vel slope (Supplemental Figure 2.4B), consistent with human observations and our data at a

single stimulation setting (Figure 2.2C). We next calculated a similar metric for dyskinesia: the slope of the correlation between  $p_i^{\text{combo}}$  and the dyskinesia score (dysk slope), an indicator of tendency toward stimulation-induced dyskinesia. In line with our data from a single stimulation setting (Figure 2.2D), we observed that electrodes closer to the internal capsule tended to have higher dysk slopes (Supplemental Figure 2.4C). Finally, and perhaps most excitingly, we found no correlation between vel slope and dysk slope (Supplemental Figure 2.4D). These findings suggest that despite a shared correlation with  $p_i^{\text{combo}}$ , improved DBS efficacy and the vulnerability to dyskinesias may be dissociable.

Optimizing patient DBS parameters is common, but extensive controlled testing is challenging in a clinical setting. Indeed, few studies have explored parameter space while measuring quantitative outcomes. However, one human study tested a subset of the parameter space (voltage, frequency, and pulse width) described here, using hand tapping as a measure of bradykinesia<sup>13</sup>. We reanalyzed this data to determine if a similar relationship between stimulation parameters and therapeutic effects governs STN DBS in PD patients. Based on parameter combinations tested in all 12 patients within a range equivalent to those tested in mice (Supplemental Figure 2.2B, Supplemental Table 2.3), we calculated a constant-voltage version of  $p_i^{\text{combo}}$  ( $p_v^{\text{combo}} = \text{voltage}^2 * \text{frequency} * \text{pulse width}$ ) and estimated efficacy. We found that tapping speed was strongly correlated with  $p_v^{\text{combo}}$  (Figure 2.3F). These human results are consistent with our findings in parkinsonian mice: STN DBS efficacy for bradykinesia (as measured by locomotor velocity) scales linearly with a combined metric incorporating all three stimulation parameters.

## Discussion

Though STN DBS has provided symptomatic relief to PD patients for over two decades, ideal parameters for DBS, as well as their underlying therapeutic mechanisms, are still unclear. We used a set of custom-built tools to create a model of STN DBS in hemiparkinsonian mice, and leveraged this model to rigorously explore the parameter space for effective DBS. We found that STN DBS is not only effective in restoring near-normal levels of locomotion in parkinsonian mice, but that it recapitulates many key features of STN DBS in PD patients. We found low frequency DBS could be effective, provided pulse width and current amplitude were adjusted to compensate. Indeed, behavioral effectiveness depended linearly on a combination of all three parameters,  $p_i^{\text{combo}}$ , suggesting a much larger and more predictable parameter space than previously assumed. Finally, we found that a similar metric strongly predicted relief of bradykinesia in a human DBS dataset; however, due to differences in brain size, parkinsonism features, and the stimulation devices used between humans and mice, further human studies are clearly needed.

Our findings support the hypothesis that stimulation frequency does not uniquely predict DBS efficacy; indeed, multiple recent human studies also report low frequency DBS is effective<sup>26,27</sup>. This relationship may not have been detected previously due to practical clinical barriers to systematic study of parameter space as well as outcome measures used. Utilizing a model such as ours facilitates a wider and more standardized exploration of parameter space, which can be used to generate new hypotheses for optimal human treatment.



We hope the STN DBS mouse model presented here can serve as a new platform, allowing the use of the powerful mouse genetic toolbox to investigate how STN DBS modifies activity patterns in basal ganglia-thalamocortical circuits. These tools, such as genetically-encoded calcium and voltage sensors, as well as optical and chemical manipulators of neural activity, will allow causal investigation of DBS therapeutic mechanisms in the future, complementing ongoing groundbreaking work in patients, non-human primates, and rat models.

## **Methods**

### **Study approval**

All the animal studies were approved by the Institutional Animal Care and Use Committee of the University of California San Francisco.

### **Experimental design**

The aim of this study was to develop a model of STN DBS in hemiparkinsonian mice, and to evaluate the parameter space for effective STN DBS in this model. Our hypothesis, based on pilot studies, was that the parameter space would mirror the space described for human PD patients and depend largely upon the frequency of stimulation rather than pulse width or current amplitude. Experiments were designed based on power analyses that indicated a minimum of 10 mice would be necessary to detect behavioral differences between effective and ineffective stimulation parameters. Stimulation parameter order was randomized across all mice and predefined quantitative measures of motor performance were used to assess changes in parkinsonian symptoms. Though we tested 11 parkinsonian mice in this study, postmortem tissue for anatomical confirmation of the stimulation site could not be recovered from two mice, and thus their behavioral data was

excluded from the study. To verify that 1- and 10-minute stimulation epochs evoked similar increases in movement, an additional cohort of 7 mice were evaluated. A third cohort of 5 mice was used in Figure 2.3B-D to determine how velocity scales with pulse width or current while all other parameters are held constant.

### **Surgical procedures**

All surgical procedures were performed stereotactically on 3-6 month old C57BL/6 mice (Jackson Laboratory). Anesthesia was induced with intraperitoneal (IP) injection of ketamine/xylazine (0.1mL, 1mg/mL) and maintained with 0.5-1% inhaled isoflurane. The neurotoxin 6-hydroxydopamine (6-OHDA, 1 $\mu$ L, 5mg/mL in normal saline) was injected unilaterally in the medial forebrain bundle (MFB, -1.0 AP, -1.0 ML, 4.9 DV). Desipramine (0.2mL, 2.5mg/mL) was injected intraperitoneally (IP) just prior to surgery to reduce uptake by serotonergic and noradrenergic neurons in the MFB. This procedure resulted in near-complete loss of ipsilateral dopaminergic innervation of the striatum and severe hemiparkinsonism. After surgery, animals received analgesic agents and IP saline. During the first week of recovery, cages were placed on a heating pad and animals received supplementary IP saline, gel nutritional supplements, and softened food. A minimum of two weeks following dopamine depletion, mice were implanted with a 6-lead bipolar stimulating electrode array in the ipsilesional STN (-1.4 AP, -1.65 ML, 4.5 DV). Mice recovered for at least 1 additional week before stimulation testing began.

### **Electrode fabrication**

Six-lead bipolar stimulating electrodes were constructed by twisting together and heating 6 stainless steel 76.2 $\mu$ m coated wires (A-M Systems). The six untwisted ends were then

stripped using a razor blade and pressure fit into female Millmax connectors. Each electrode was tested for short circuits prior to implantation.

### **Electrical stimulation**

An isolated constant current bipolar stimulator (WPI) was used to deliver electrical stimuli. The stimulator had a maximum voltage supply of >100 volts, a rise time of 6 $\mu$ s, and a built-in alarm indicating when the voltage limit was exceeded. We calculated that even at the highest settings used here we would not reach more than 80% of the total voltage available (ensuring accurate current delivery), a conclusion supported by the fact that the built-in voltage limit alarm did not sound during any of the experiments. The timing of stimuli was controlled by TTL input from an Arduino. Maximum current amplitude was set at 400 $\mu$ A, based on pilot experiments in which seizures occurred in some mice at or above this level.

### **Optimal stimulation electrode determination**

Optimal stimulation electrode pairs were determined following STN DBS implantation based on the behavioral response of each pair in the open field setting. Each of the 3 electrode pairs were stimulated at standard settings (200 $\mu$ A, 60 $\mu$ s pulse-width, 120Hz) for 1 minute, flanked by 1 minute stim-off rest periods. The electrode pair eliciting the largest increase in velocity during stimulation epochs was used for all subsequent studies (Supplemental Figure 2.1D). In one mouse, a short developed between its optimal electrode pair in the interval between early and late stimulation phases, so the electrode pair was switched during the late phase to another pair that had shown similar efficacy to the optimal pair during initial characterization.

## Open field behavior

Following optimal electrode pair selection, efficacy of STN DBS in parkinsonian mice was assessed in the open field (a transparent acrylic cylinder with a diameter of 25cm) during 11-minute trials in which 1-minute epochs of stimulation were alternated with 1-minute epochs of no stimulation (rest). Every trial began and ended with a rest epoch, resulting in a total of 5 stimulation epochs and 6 rest epochs per trial. The parameters of stimulation were consistent within each trial and varied randomly between trials. Possible parameter combinations were chosen from a list of 81 parameters, half of which were pseudorandomly generated (current drawn from 0 to 300 $\mu$ A, frequency drawn from 0 to 200Hz, pulse width drawn from 0 to 120 $\mu$ s, all in integer increments) while the other half were deliberately selected. All mice received at least 1 trial with each parameter. A composite metric,  $p_i^{\text{combo}}$ , was calculated for each parameter combination using the formula  $p_i^{\text{combo}} = [\text{current}^2 * \text{frequency} * \text{pulse width}]^{23}$ .

Dyskinesia during stimulation and rest epochs was quantified using a modified version of the abnormal involuntary movements (AIM) scoring method<sup>18</sup>. Dyskinesia was monitored online by one unblinded rater, and a subset of videos (222 minutes) were re-scored offline by one blinded rater to ensure low inter-rater variability (average difference between raters' individual AIM scores = 0.05 +/- 0.009). Dyskinesia was quantified in one-minute increments during each trial, with axial, limb, and orofacial body segments rated on a scale of 0-3 each. A score of 0 indicates no abnormal movement, while a score of 3 indicates abnormal movements during the entire minute-long epoch. The scores are then summed, for a maximum score of 9 per epoch.

Following each trial, video-tracking software (Noldus Ethovision) was used to calculate the velocity, percent time moving, and rotational bias of each mouse (calculated as rotational bias = ipsilateral rotations / (ipsilateral rotations + contralateral rotations), and all metrics were compared between stimulation and rest epochs. As the dyskinesias observed in our study largely did not provoke changes in the center of mass of the mouse they did not contaminate the calculation of velocity and thus no additional processing was required to separate the two.

The onset of stimulation-induced changes in velocity was defined as the first time point during a stimulation bout in which the velocity was three standard deviations above the mean of the pre-stim period. The offset of stimulation-induced changes in velocity was defined as the first time point during each post-stimulation period in which velocity returned to the mean of the respective pre-stim period.

All mice initially experienced 31 of the 81 parameters within a 1 to 3-week period, approximately 1 month following implantation (early DBS). They then experienced the remaining 50 parameters during a 3-week period, approximately 3 months following implantation (late DBS), in order to assess changes in DBS efficacy.

For 10-minute stimulation epochs performed in a separate cohort of 7 mice (Supplemental Figure 2.1E), trials lasted for 30 minutes and consisted of a 10-minute pre-stim period, followed by a 10-minute stim period, and concluded with a 10-minute post-stim period. To account for habituation-related declines in spontaneous movement for these longer sessions, velocity during 120Hz stimulation was normalized to the average velocity during a 30-minute no-stimulation trial. Standard error for this normalized velocity was calculated through propagation of error.

## **Locomotion in healthy mice**

Open field locomotor data for healthy, nonparkinsonian controls was obtained from a separate cohort of mice with intracranial implants and headstage cables, so as to closely replicate the potential effects of tethering in STN DBS mice. Tracking data (Noldus) was analyzed in the same fashion as in parkinsonian mice: nonparkinsonian controls were only analyzed for movement metrics within the first 10 minutes of recording.

## **Human data**

All human data were estimated from bar graphs provided by Moro, et al<sup>13</sup>. In order to analyze human data in as similar a fashion as possible to the mouse data collected here, only parameter combinations in which all 12 patients had participated were used. Additionally, only parameters that fell within a range equivalent to those tested in mice were used (frequency between 0 and 200Hz and pulse width between 0 and 120 $\mu$ s). For determining voltage range (since our mice were tested using constant current), we used a range from 0V to twice as high as the patient average for current clinical settings (since our maximum tested current, 400 $\mu$ A, was twice our estimate for standard human parameters, 200 $\mu$ A, and since current and voltage scale linearly). Thus, voltages between 0 and 6.2V were considered. To adjust  $p_i^{\text{combo}}$  for constant voltage rather than constant current, we used the formula  $p_v^{\text{combo}} = [\text{voltage}^2 * \text{frequency} * \text{pulse width}]$ .

## **DBS model**

The models for DBS efficacy were developed using the regressions generated in Figure 2.3E (for Supplemental Figure 2.3A-D) and Supplemental Figure 2.2C (for Supplemental Figure 2.3E-H) to calculate predicted velocity for parameters within the space shown

(current from 0-400 $\mu$ A in 20 $\mu$ A increments, frequency from 0-200Hz in 10Hz increments, and pulse width from 0-200 $\mu$ s in 10 $\mu$ s increments).

### **Statistics**

All behavioral data recorded with video tracking (Noldus Ethovision) was exported to Matlab (Mathworks) for offline analysis. Statistical differences between stimulation parameters were assessed using one-way repeated-measures ANOVA, followed by post hoc comparisons using Tukey's Honest Significant Difference procedure.  $P_{\text{adjusted}}$  reported for ANOVAs is a p-value with the most conservative lower bound adjustment, as calculated by Matlab. Linear correlations and adjusted R-squared values were calculated in Matlab by fitting data to a linear model. The generalized linear model was created in Matlab using a normal distribution.

### **Histology**

Accurate targeting of STN DBS electrodes and successful depletion of dopaminergic projections to the striatum were confirmed histologically following perfusion. Two mice, out of the original cohort of 11, were excluded from analysis as postmortem tissue (confirming electrode localization) could not be recovered. Mice were deeply anesthetized with IP ketamine/xylazine (1 ml, 1mg/mL). In order to aid in locating STN DBS electrode tips in postmortem tissue, we electrolytically lesioned the two leads used for behavioral experiments with 150 $\mu$ A of monopolar direct current for 5 seconds, just prior to transcardial perfusion with paraformaldehyde (PFA). The brain was dissected from the skull, post-fixed overnight in 4% PFA, then stored in 30% sucrose at 4°C. Brains were then sliced in 30  $\mu$ m sections on a freezing microtome (Leica) and dopamine depletion was verified via tyrosine hydroxylase (TH) immunohistochemistry. Briefly, sections were

washed in PBS (5x10 minutes) and blocked in normal donkey serum (NDS)/0.1% Triton-X (1hr at room temperature, RT), followed by incubation in primary antibody (Pel-Freez rabbit anti-TH, 1:1000 at 4°C overnight) and secondary antibody (donkey anti-rabbit 647 nm, Jackson ImmunoResearch, 1:500 in NDS at RT for 2hrs). Following mounting on glass slides (Vectashield Mounting Medium), sections were imaged in the Cy5 (excitation 650nm, emission 684nm) channel and stitched fluorescence images were taken on a Nikon 6D conventional wide-field microscope at 4-10X, using custom software (UCSF Nikon Imaging Center). Coordinates of mouse DBS electrodes were determined from histological images using a standard mouse brain atlas (Paxinos and Franklin). Center coordinates for the dorsal border pyramidal tract were determined in a similar way, and distance between this point and the coordinates of the electrode for each mouse was calculated using Euclidean distance.

### **Contributions**

JSS and ABN designed experiments. JSS built all experimental components (commutator, stimulation electrodes) and performed all experiments and analyses. JSS and ABN wrote the manuscript.

### **Acknowledgements**

The authors would like to acknowledge P. Starr, J. Ostrem, K. Bender, D. Ron, K. Kay, AL Benabid, and members of the Nelson Lab for providing advice and feedback on the manuscript. We thank R. Brakaj and C. Bair-Marshall for technical support. This work was supported by the NINDS (K08 NS081001, ABN). ABN is the Richard and Shirley Cahill Endowed Chair in Parkinson's Disease Research.



## References

1. Ahlskog, J. E. & Muentner, M. D. Frequency of levodopa-related dyskinesias and motor fluctuations as estimated from the cumulative literature. *Mov. Disord. Off. J. Mov. Disord. Soc.* **16**, 448–458 (2001).
2. Obeso, J. A. *et al.* Surgical treatment of Parkinson's disease. *Baillieres Clin. Neurol.* **6**, 125–145 (1997).
3. Wichmann, T. & DeLong, M. R. Deep Brain Stimulation for Neurologic and Neuropsychiatric Disorders. *Neuron* **52**, 197–204 (2006).
4. Dayal, V., Limousin, P. & Foltynie, T. Subthalamic Nucleus Deep Brain Stimulation in Parkinson's Disease: The Effect of Varying Stimulation Parameters. *J. Park. Dis.* **7**, 235–245.
5. McGregor, M. M. & Nelson, A. B. Circuit Mechanisms of Parkinson's Disease. *Neuron* **101**, 1042–1056 (2019).
6. Chiken, S. & Nambu, A. Disrupting neuronal transmission: mechanism of DBS? *Front. Syst. Neurosci.* **8**, (2014).
7. Eusebio, A. *et al.* Effects of low-frequency stimulation of the subthalamic nucleus on movement in Parkinson's disease. *Exp. Neurol.* **209**, 125–130 (2008).
8. Reich, M. M. *et al.* Short pulse width widens the therapeutic window of subthalamic neurostimulation. *Ann. Clin. Transl. Neurol.* **2**, 427–432 (2015).

9. Moran, A., Stein, E., Tischler, H., Bebelovsky, K. & Bar-Gad, I. Dynamic Stereotypic Responses of Basal Ganglia Neurons to Subthalamic Nucleus High-Frequency Stimulation in the Parkinsonian Primate. *Front. Syst. Neurosci.* **5**, (2011).
10. Hashimoto, T., Elder, C. M., Okun, M. S., Patrick, S. K. & Vitek, J. L. Stimulation of the subthalamic nucleus changes the firing pattern of pallidal neurons. *J. Neurosci.* **23**, 1916–1923 (2003).
11. Gradinaru, V., Mogri, M., Thompson, K. R., Henderson, J. M. & Deisseroth, K. Optical Deconstruction of Parkinsonian Neural Circuitry. *Science* **324**, 354–359 (2009).
12. Brocker, D. T. *et al.* Optimized temporal pattern of brain stimulation designed by computational evolution. *Sci. Transl. Med.* **9**, eaah3532 (2017).
13. Moro, E. *et al.* The impact on Parkinson's disease of electrical parameter settings in STN stimulation. *Neurology* **59**, 706–713 (2002).
14. Zheng, Z. *et al.* Stimulation-induced dyskinesia in the early stage after subthalamic deep brain stimulation. *Stereotact. Funct. Neurosurg.* **88**, 29–34 (2010).
15. Greenhouse, I. *et al.* Stimulation at dorsal and ventral electrode contacts targeted at the subthalamic nucleus has different effects on motor and emotion functions in Parkinson's disease. *Neuropsychologia* **49**, 528–534 (2011).
16. Tommasi, G. *et al.* Pyramidal tract side effects induced by deep brain stimulation of the subthalamic nucleus. *J. Neurol. Neurosurg. Psychiatry* **79**, 813–819 (2008).

17. Li, Q. *et al.* Therapeutic Deep Brain Stimulation in Parkinsonian Rats Directly Influences Motor Cortex. *Neuron* **76**, 1030–1041 (2012).
18. Cenci, M. A. & Lundblad, M. Ratings of L-DOPA-induced dyskinesia in the unilateral 6-OHDA lesion model of Parkinson's disease in rats and mice. *Curr. Protoc. Neurosci.* Chapter 9, Unit 9.25 (2007).
19. Hamani, C., Saint-Cyr, J. A., Fraser, J., Kaplitt, M. & Lozano, A. M. The subthalamic nucleus in the context of movement disorders. *Brain* **127**, 4–20 (2004).
20. Nambu, A., Takada, M., Inase, M. & Tokuno, H. Dual somatotopical representations in the primate subthalamic nucleus: evidence for ordered but reversed body-map transformations from the primary motor cortex and the supplementary motor area. *J. Neurosci.* **16**, 2671–2683 (1996).
21. Plaha, P., Ben-Shlomo, Y., Patel, N. K. & Gill, S. S. Stimulation of the caudal zona incerta is superior to stimulation of the subthalamic nucleus in improving contralateral parkinsonism. *Brain J. Neurol.* **129**, 1732–1747 (2006).
22. Blomstedt, P. *et al.* Deep brain stimulation in the caudal zona incerta versus best medical treatment in patients with Parkinson's disease: a randomised blinded evaluation. *J. Neurol. Neurosurg. Psychiatry* **89**, 710–716 (2018).
23. Koss, A. M., Alterman, R. L., Tagliati, M. & Shils, J. L. Calculating total electrical energy delivered by deep brain stimulation systems. *Ann. Neurol.* **58**, 168–168 (2005).

24. Wagle Shukla, A., Zeilman, P., Fernandez, H., Bajwa, J. A. & Mehanna, R. DBS Programming: An Evolving Approach for Patients with Parkinson's Disease. *Parkinson's Disease* <https://www.hindawi.com/journals/pd/2017/8492619/> (2017)  
doi:10.1155/2017/8492619.
25. Satzer, D., Lanctin, D., Eberly, L. E. & Abosch, A. Variation in Deep Brain Stimulation Electrode Impedance over Years Following Electrode Implantation. *Stereotact. Funct. Neurosurg.* **92**, 94–102 (2014).
26. Khoo, H. M. *et al.* Low-frequency subthalamic nucleus stimulation in Parkinson's disease: a randomized clinical trial. *Mov. Disord. Off. J. Mov. Disord. Soc.* **29**, 270–274 (2014).
27. Blumenfeld, Z. *et al.* Sixty Hertz Neurostimulation Amplifies Subthalamic Neural Synchrony in Parkinson's Disease. *PLoS ONE* **10**, (2015).

**Figure 2.1**

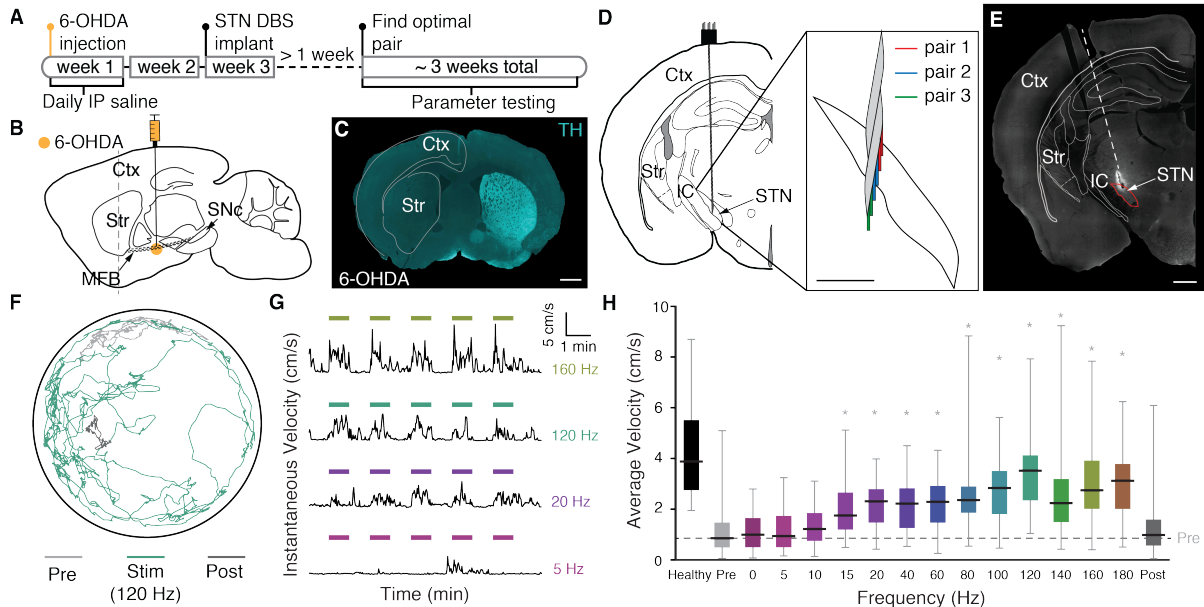


**Figure 2.1. Subthalamic nucleus deep brain stimulation (STN DBS) alleviates bradykinesia in parkinsonian mice across a wide range of frequencies.**

**(A)** Experimental timeline. **(B)** Sagittal schematic showing unilateral 6-OHDA medial forebrain bundle (MFB) injection. **(C)** Representative coronal section immunostained for tyrosine hydroxylase (TH) showing ipsilateral depletion of striatal TH (scale bar = 750 $\mu$ m). **(D-E)** Coronal schematic (D) and histological section (E); scale bars = 250 and 750 $\mu$ m) showing ipsilesional STN targeting of DBS electrode (dotted white line and terminal electrolytic lesion). **(F)** Representative open field movement before, during, and after 120Hz STN DBS in a parkinsonian mouse (5 minutes each). **(G)** Representative raw velocity traces over standard 11-minute trials, consisting of five 1-minute bouts of 5Hz, 20Hz, 120Hz, and 160Hz STN DBS interleaved with six 1-minute rest bouts. **(H)** Average velocity of parkinsonian mice during stimulation epochs across frequencies with constant pulse width (60 $\mu$ s) and constant current (200 $\mu$ A). Healthy refers to nonparkinsonian mice. Pre and post refer to 30 seconds before and after stimulation. Box extends from 25<sup>th</sup> to 75<sup>th</sup> percentile, median is indicated by horizontal line. Whiskers represent max and min values. (N=9 healthy mice, N=9 parkinsonian mice; Significance determined by one-way repeated measures ANOVA followed by Tukey's Honest Significant Difference test, \* p<.05 compared to pre-stim period). IP=intraperitoneal, Ctx=cortex, Str=striatum, SNc=substantia nigra pars compacta, IC=internal capsule, STN=subthalamic nucleus.

**Figure 2.2**

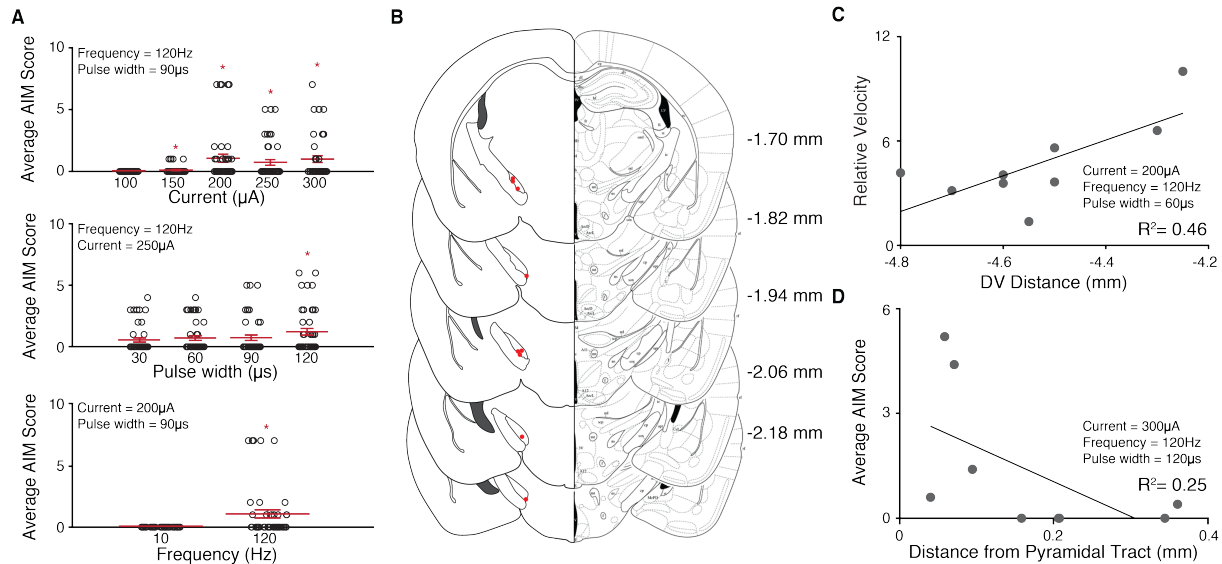


**Figure 2.2. STN DBS in parkinsonian mice recapitulates key features of human DBS.**

**(A)** Average abnormal involuntary movement (AIM) score of parkinsonian mice during 1-minute stimulation epochs as a function of current (Top), pulse width (Middle), or frequency (Bottom), holding the other two parameters constant (N=9, 5 trials per mouse per condition). **(B)** Stimulation sites across all mice, as determined postmortem (N=9; red dots). **(C)** Correlation between dorsoventral (DV) stimulation site and velocity increases for individual mice at standard parameters (N=9). **(D)** Correlation between the stimulation site-pyramidal tract distance and average AIM score for individual mice at the parameter setting shown (N=9). Significance determined by one-way repeated measures ANOVA (performed on all stimulation parameters shown in (A)) followed by Tukey's Honest Significant Difference test, \*  $p < .05$  compared to lowest stimulation setting. N=mice.

**Figure 2.3**

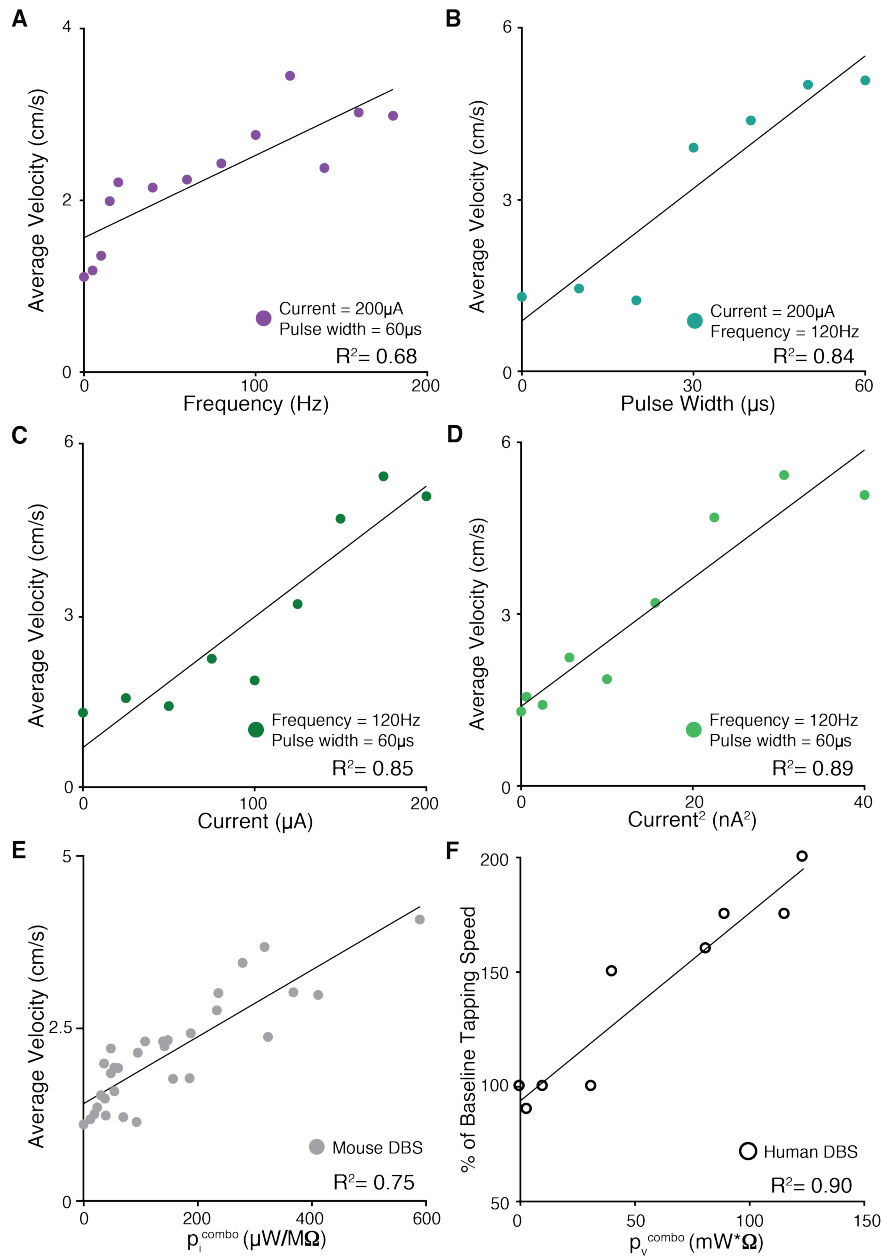


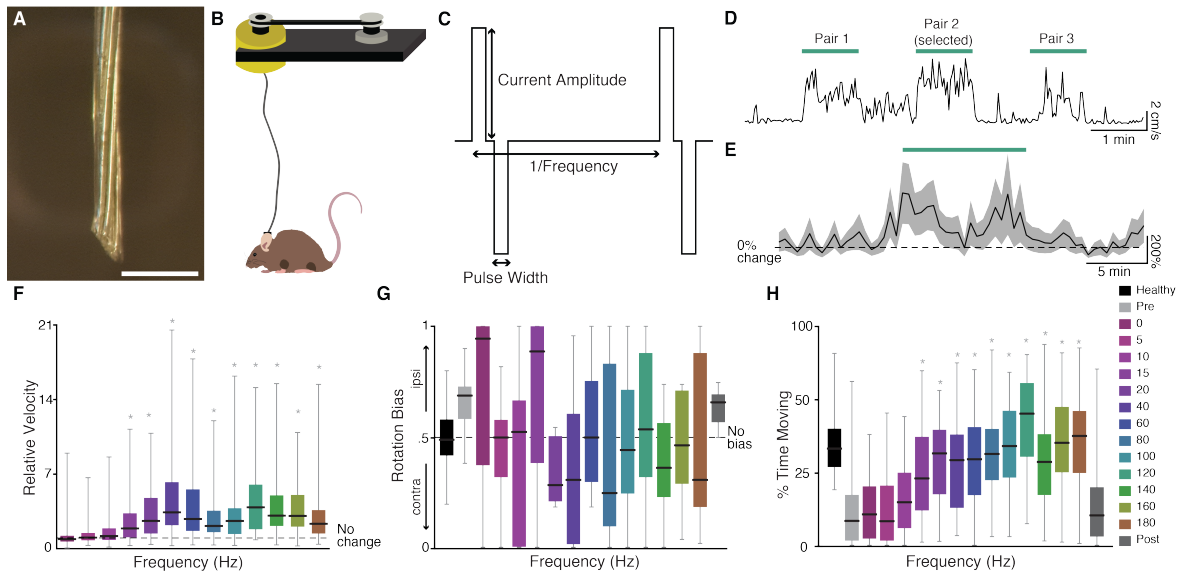
**Figure 2.3. Effectiveness of STN DBS depends linearly on a composite stimulation parameter metric,  $p^{combo}$ .**

(A-D) In parkinsonian mice, correlation of velocity during DBS with (A) frequency (N=9), (B) pulse width (N=5), (C) current (N=5), or (D) current-squared (N=5), holding the other two parameters constant. (E) In parkinsonian mice, correlation of velocity with  $p_i^{combo}$  following DBS (31 conditions, N=9). (F) In humans, correlation of % of baseline tapping speed with  $p_v^{combo}$  (9 conditions, N=12) during DBS (reanalyzed from Moro, et al<sup>13</sup>).

N=mice or humans. Each point represents an average across subjects and trials for a given condition.



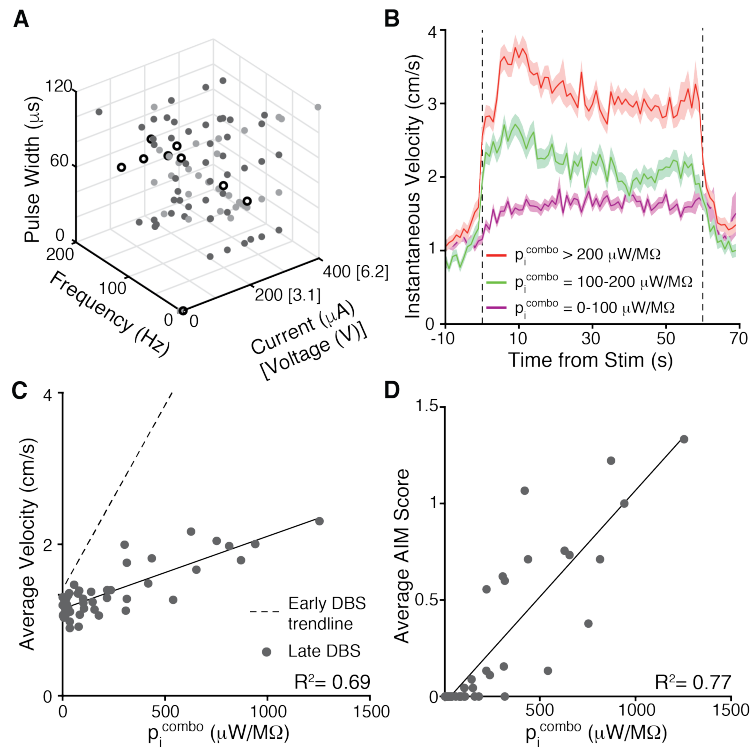
## Supplemental Figure 2.1



### Supplemental Figure 2.1. STN DBS improves multiple movement metrics in hemiparkinsonian mice.

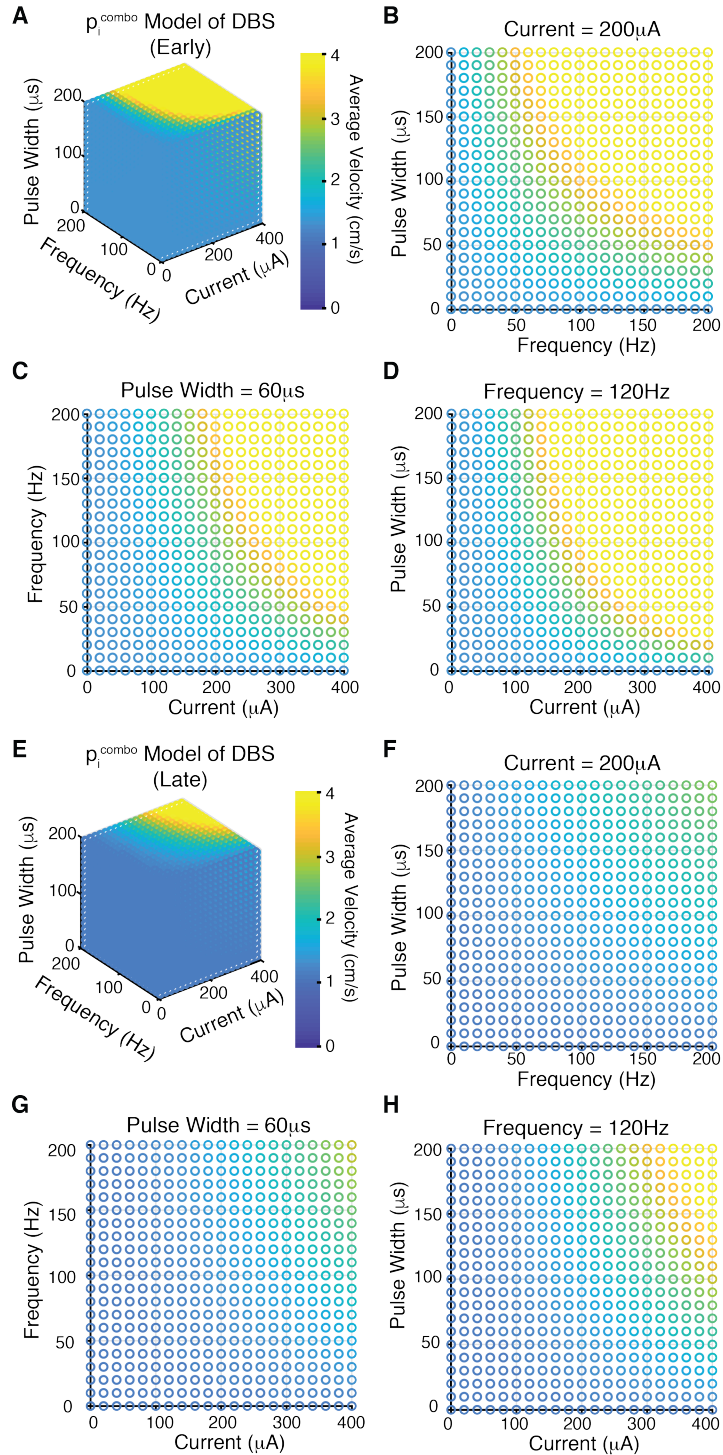
**(A)** Photograph of DBS electrodes implanted in parkinsonian mice (scale bar = 1mm). **(B)** Schematic of experimental behavioral setup, including custom motorized commutator. **(C)** Diagram of bipolar, biphasic stimulation delivered during experimentation. **(D)** Sample raw velocity trace for optimal electrode pair determination. **(E)** Normalized velocity during 10 minute stimulation epochs (green bar). Dark line indicates averages, while lighter shading indicates  $\pm$  SEM (N=7). **(F-H)** Relative velocity (F), rotational bias (G), and percent time moving (H) of parkinsonian mice during stimulation (1min) at the denoted frequencies, with pulse width (60 $\mu$ s) and current (200 $\mu$ A) held constant. Pre and post refer to 30 seconds before and after stimulation. Box extends from 25<sup>th</sup> to 75<sup>th</sup> percentile, median is indicated by horizontal line. Whiskers represent max and min values. (N=9 for healthy, N=9 for parkinsonian). Significance determined by one-way repeated measures ANOVA followed by Tukey's Honest Significant Difference test, \*  $p < .05$  compared to pre-stim period. N=mice.

## Supplemental Figure 2.2



**Supplemental Figure 2.2. Both dyskinesia and DBS efficacy scale with  $p_i^{\text{combo}}$ .** **(A)** Distribution of early (31 total, light grey dots) and late (50 total, dark grey dots) mouse and human (9 total, open circles) DBS parameters. **(B)** Instantaneous velocity during stimulation for parameters within the indicated  $p_i^{\text{combo}}$  ranges. Dark lines indicate averages, while lighter shadings indicate  $\pm$  SEM. **(C)** Correlation of velocity with  $p_i^{\text{combo}}$  (50 conditions, N=9) in late DBS (~2 months after early DBS). **(D)** Correlation of average AIM score with  $p_i^{\text{combo}}$  (50 conditions, N=9). N=mice. Each point represents an average across subjects and trials for a given condition.

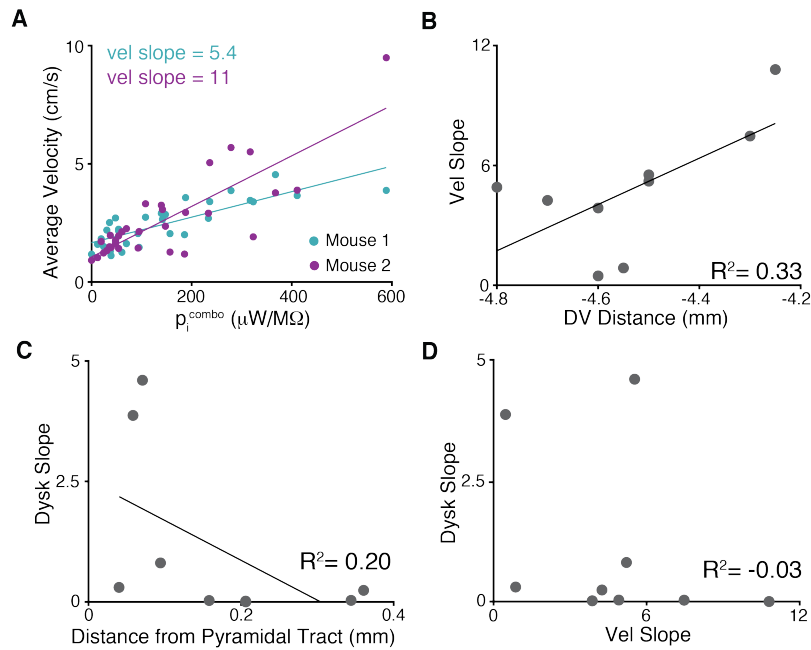
# Supplemental Figure 2.3



**Supplemental Figure 2.3. Modeling DBS using  $p_i^{\text{combo}}$  predicts the therapeutic parameter space.**

**(A)** 3-D representation of STN DBS parameter space based on the early regression generated from data in Figure 2.3E. **(B-D)** Cross-sections of STN DBS parameter space from (A) at constant current (B), pulse width (C), and frequency (D). **(E)** 3-D representation of STN DBS parameter space based on the late regression generated from data in Supplemental Figure 2.2C. **(F-H)** Cross-sections of STN DBS parameter space from (E) at constant current(F), pulse width (G), and frequency (H).

## Supplemental Figure 2.4



### Supplemental Figure 2.4. Movement velocity and dyskinesia relationships to $p_i^{\text{combo}}$ by stimulation sites across individual mice.

**(A)** Correlations between velocity and  $p_i^{\text{combo}}$  in two sample mice (31 conditions) illustrating differences in the slope of the correlation (vel slope). **(B)** Correlation between dorsoventral (DV) stimulation location and vel slope across individual mice (N=9). **(C)** Correlation between the stimulation site-pyramidal tract distance and dysk slope across individual mice (N=9). **(D)** Correlation between vel slope and dysk slope across individual mice (N=9). N=mice.

## Supplemental Table 2.1

### Supplemental Table 2.1. Early DBS Parameters.

Table showing the parameters used for early DBS testing.

Current ( $\mu\text{A}$ )	Frequency (Hz)	Pulse Width ( $\mu\text{s}$ )
100	100	40
100	120	60
100	120	120
150	120	60
175	20	50
175	40	50
200	5	60
200	10	60
200	10	120
200	15	60
200	20	60
200	40	60
200	60	60
200	60	100
200	80	60
200	100	60
200	120	20
200	120	40

Current ( $\mu\text{A}$ )	Frequency (Hz)	Pulse Width ( $\mu\text{s}$ )
200	120	60
200	160	60
200	180	60
225	80	80
250	10	60
250	60	40
250	140	70
300	5	120
300	10	60
300	10	120
400	1	120
0	0	0

## Supplemental Table 2.2

### Supplemental Table 2.2. Late DBS Parameters.

Table showing the parameters used for late DBS testing.

Current ( $\mu\text{A}$ )	Frequency (Hz)	Pulse Width ( $\mu\text{s}$ )
10	88	46
10	170	113
13	19	99
35	100	116
42	84	110
83	109	115
100	10	30
100	10	60
100	10	90
100	10	120
100	120	30
100	120	90
102	117	27
118	131	20
147	89	78
150	10	30
150	10	60
150	10	90



Current ( $\mu\text{A}$ )	Frequency (Hz)	Pulse Width ( $\mu\text{s}$ )
150	10	120
150	120	90
150	120	120
200	10	30
200	10	90
200	120	30
200	120	90
204	131	19
204	152	89
209	63	114
212	6	33
213	151	33
230	159	22
238	192	79
245	182	15
250	10	30
250	10	90
250	10	120
250	120	30
250	120	60
250	120	90

Current ( $\mu\text{A}$ )	Frequency (Hz)	Pulse Width ( $\mu\text{s}$ )
250	120	120
288	97	96
290	31	117
300	10	30
300	10	90
300	120	30
300	120	60
300	120	90
300	120	120

## Supplemental Table 2.3

### Supplemental Table 2.3. Human DBS Parameters.

Table showing the parameters used in human DBS testing.

Voltage (V)	Frequency (Hz)	Pulse Width ( $\mu$ s)
1	155	65
2	155	65
3.1	5	65
3.1	50	65
3.1	130	65
3.1	185	65
0	0	0
3.5	155	65
3.1	155	60

**Chapter 3:**

**Levodopa and STN Deep Brain Stimulation Relieve  
Parkinsonian Motor Symptoms with Opposing  
Changes in Basal Ganglia Activity<sup>‡</sup>**

<sup>‡</sup>A version of this chapter is currently in submission as Schor JS, Gonzalez Montalvo I, Spratt PWE, Brakaj RJ, Bender KJ, and Nelson AB. Levodopa and STN Deep Brain Stimulation Relieve Parkinsonian Motor Symptoms with Opposing Changes in Basal Ganglia Activity.

# **Levodopa and STN Deep Brain Stimulation Relieve Parkinsonian Motor Symptoms with Opposing Changes in Basal Ganglia Activity**

## **Abstract**

Levodopa and subthalamic nucleus deep brain stimulation (STN DBS) are two common treatments for the motor symptoms of Parkinson's disease (PD). While both treatments had been hypothesized to inhibit basal ganglia output activity, it is currently unknown whether they act through similar or distinct mechanisms. To investigate these two possibilities, we performed calcium imaging in parkinsonian mice during treatment with levodopa and STN DBS. Using this approach, we found, as predicted, that levodopa inhibits activity in the substantia nigra pars reticulata (SNr). However, we found that STN DBS increases activity in the STN and SNr. Furthermore, both optical inhibition of SNr neurons and excitation of STN neurons provide behavioral benefits that mirror those of levodopa and STN DBS, respectively. Together, these results suggest bidirectional changes in basal ganglia activity can alleviate PD motor symptoms, which may both refine basal ganglia models and inform development of new neuromodulatory therapies.

## Introduction

Parkinson's disease (PD) is a neurodegenerative disorder characterized by the loss of midbrain dopamine neurons, and manifests with profound motor deficits such as bradykinesia and tremor. PD patients are often treated with either dopamine replacement therapy (e.g. the dopamine precursor levodopa), subthalamic nucleus deep brain stimulation (STN DBS), or a combination of the two. While both levodopa and STN DBS can relieve motor symptoms, our ability to improve either treatment modality, or to assess their potential for treating other diseases, is hampered by a lack of understanding of their underlying mechanisms of action.

Both levodopa and STN DBS are hypothesized to modify neural activity in the basal ganglia, a series of interconnected subcortical nuclei whose function is known to be disrupted in PD. Traditional models of the basal ganglia posit that loss of dopaminergic input to the basal ganglia in PD leads to increased activity in the basal ganglia output nuclei (globus pallidus pars interna, GPi; substantia nigra pars reticulata, SNr) and reduced movement<sup>1,2</sup>. These models also predict hyperactivity in the major excitatory input to GPi/SNr, the STN. This hypothesis has largely been borne out in both PD patients and animal models of PD, though some exceptions do exist<sup>3</sup>.

Dopamine replacement therapy is hypothesized to normalize basal ganglia function by decreasing activity at the level of both STN and GPi/SNr. Single-unit electrophysiology in GPi/SNr of rodents, non-human primates (NHPs), and humans have largely reinforced this notion<sup>4-7</sup>. However, electrophysiological studies of the STN have been far more variable, showing increases<sup>8</sup>, decreases<sup>9</sup>, or no change in activity in response to dopamine replacement<sup>10</sup>.

Initially, STN DBS was also thought to act by inhibiting basal ganglia activity. As it had long been known that STN lesions were therapeutic in PD<sup>11,12</sup>, STN DBS was developed as a “reversible lesion”. However, whether STN DBS actually inhibits basal ganglia activity has become increasingly unclear. One reason for this is that performing electrical recordings of neural activity during STN DBS is technically challenging, due to the large electrical artifacts produced during high-frequency electrical stimulation. These artifacts may obscure the accurate measurement of firing in highly active basal ganglia nuclei such as the STN, GPi, and SNr. Across multiple experimental preparations, investigators have proposed several different effects of STN DBS<sup>13</sup>. For instance, while some groups have reported the predicted inhibitory effects of STN DBS on STN and GPi/SNr<sup>14,15</sup>, others have observed excitation<sup>16,17</sup>. In fact, some have suggested that DBS acts on distant brain regions, such as the motor cortex, by antidromic stimulation. Using optogenetic DBS, these groups have found that optical stimulation of “hyperdirect” M1 neurons that project to the STN can relieve motor symptoms in parkinsonian mice<sup>18,19</sup>. These conflicting findings highlight the need to understand how electrical DBS impacts neural activity.

Here, we use region- and cell-type specific optical recording methods in an established mouse model of PD to directly compare the effects of levodopa and electrical STN DBS on activity in STN, SNr, and hyperdirect M1 neurons. As in humans, we find that both levodopa and STN DBS improve slowing of movement, or bradykinesia, in the mouse model. As predicted, levodopa inhibits activity at the level of basal ganglia output (SNr). STN DBS, however, *increases* activity in both the STN and SNr. Furthermore,

optical inhibition of SNr and optical excitation of STN, which mimic the most salient effects of levodopa and STN DBS, respectively, improve bradykinesia in parkinsonian mice. Taken together, these results suggest these two therapies act through distinct and seemingly opposing neural mechanisms.

## **Results**

### **Both Levodopa and STN DBS relieve parkinsonism in mice**

While levodopa and STN DBS have been utilized in several animal models of PD, their behavioral effects have not been directly compared in mice. We used the unilateral 6-OHDA mouse model of PD, which in our previous work shows reduced movement velocity (~1 cm/s vs ~4 cm/s in healthy controls) and an ipsilesional rotational bias<sup>20</sup>. To test whether levodopa and STN DBS similarly improve movement parameters, we measured the open-field locomotion and rotational bias of 6-OHDA-treated mice during administration of either levodopa (5 mg/kg i.p.) or electrical STN DBS (bipolar, biphasic stimulation at 60 or 100 Hz with a 60  $\mu$ s pulse-width and an amplitude of 200  $\mu$ A). Levodopa reliably increased movement velocity (Figure S3.1A-C; N=32, LD vs pre/post:  $p < 0.001$ ) and produced a contralesional rotation bias (Figure S3.1D; LD vs pre/post:  $p < 0.001$ ). Additionally, in a minority of mice, levodopa evoked moderate dyskinesias (Figure S3.1E; AIM score  $0.66 \pm 0.2$ ), as has been previously reported<sup>21</sup>. Similarly, STN DBS at either 60 Hz (Figure S3.1F-H; N=39 mice) or 100 Hz (Figure S3.1K-M; N=36 mice) increased movement velocity (stim vs pre/post:  $p < 0.001$ ) and evoked moderate dyskinesias in a minority of mice (Figure S3.1J,O). However, no contralesional rotation bias was seen with STN DBS at either 60 Hz (stim vs pre/post:  $p = 0.72/0.77$ ) or 100 Hz (stim vs pre/post:  $p = 0.84/0.63$ ). Together, these results indicate that both levodopa and



STN DBS are therapeutic in parkinsonian mice, producing broadly similar effects on movement, with the notable exception of rotational behavior.

### **STN DBS consistently increases STN activity**

While treatment with levodopa and STN DBS evoked similar changes in motor behavior in parkinsonian mice, it is unknown whether they drive similar changes in STN activity. To compare the effect of levodopa and STN DBS on neural activity in the STN while minimizing DBS-related artifacts, we used calcium signals as a proxy for neural activity. We recorded bulk changes in the fluorescence of GCaMP6s, a genetically encoded calcium indicator. To target glutamatergic neurons within STN, we injected parkinsonian VGlut2-Cre mice with AAVs encoding Cre-dependent GCaMP6s, and then implanted mice with both an STN DBS device and an optical fiber (Figure 3.1A-B). We then measured changes in STN activity *in vivo* in response to treatment with levodopa or STN DBS. As in the larger cohort, levodopa increased movement velocity and evoked contralesional rotations in VGlut2-Cre mice (Figure 3.1C-D, S3.2A,D; N=9). In these sessions, STN activity overall was not significantly changed, decreasing in some sessions and increasing in others (Figure 3.1C-D, S3.2A; LD vs pre/post:  $p=0.90/0.83$ ). Injection with saline did not produce significant changes in STN activity (N=9 mice, saline vs pre/post:  $p=0.053/ p=0.97$ ), nor did it increase velocity or produce significant changes to rotation bias (Figure S3.2E). These levodopa findings, while not consistent with rate model predictions, do correspond to the variable changes seen by other groups.

We next tested whether STN DBS would produce similar changes in STN neural activity. In the same mice, we performed electrical STN DBS at either 60 or 100 Hz, which

increased movement velocity as previously observed (Figure 3.1E-H, S3.2B-D). Surprisingly, STN DBS caused a significant increase in STN calcium signals (Figure 3.1E-H, S3.2B-C; N=9 mice, stim vs pre/post:  $p < 0.001$ ). This result suggests that, contrary to classical models, neither levodopa nor STN DBS reliably inhibit STN activity, and moreover that STN DBS may *increase* STN activity.

One potential explanation for these surprising findings is that GCaMP calcium signals do not correlate with spiking activity in the high-firing STN. To examine how spiking relates to STN GCaMP signals, we performed simultaneous whole-cell current-clamp recordings and fluorescence imaging of STN neurons in *ex vivo* slices from VGlut2-Cre mice injected with GCaMP6s (Figure S3.2F,J; n=5 cells, N=2 mice). Neurons were stimulated in 1-minute epochs with current pulses at a range of frequencies, or constant current (Figure S3.2G). STN neurons showed rhythmic spiking that corresponded to the frequency of pulsatile stimulation (Figure S3.2H-I). Calcium, as measured by changes in GCaMP6s fluorescence, similarly increased during both 10 Hz and 50-60 Hz stimulation but did not increase further during 100-120 Hz stimulation (Figure S3.2K-L). These findings suggest a correlation between STN firing rates and calcium signals up to 60 Hz stimulation, and a plateau in GCaMP signal at 100-120 Hz. In response to constant current stimulation, STN neurons fired only transiently, appearing to enter depolarization block (Figure S3.2H-I). Under these circumstances, evoked calcium signals fell between those evoked by 10 and 50-60 Hz stimulation (Figure S3.2K-L). These experiments suggest that the relationship between spiking and GCaMP calcium signals may break down at very high frequencies of stimulation, or under conditions of forced depolarization

block. However, at the more moderate frequencies explored here (60 Hz), GCaMP calcium signals retain a correlation to STN firing.

### **STN DBS and levodopa have opposite effects on basal ganglia output**

Though the STN is a critical node within the basal ganglia circuit, especially in regard to dysfunction in PD and its treatment, changes in STN activity are believed to regulate motor function via excitatory projections to basal ganglia output nuclei. To assess treatment-evoked changes in activity at the level of basal ganglia output (in rodents, the SNr), we expressed GCaMP6s and implanted optical fibers in the SNr of parkinsonian mice. We either injected VGAT-Cre mice with Cre-dependent GCaMP6s (N=6 mice) or WT mice with synapsin-dependent GCaMP6s (Figure 3.2A; N=2 mice). As previously, levodopa evoked an increase in movement velocity and a contralesional rotation bias (Figure 3.2B-C, S3.3A,D). In parallel, we observed a significant decrease in SNr neural activity (Figure 3.2B-C, S3.3A; N=8 mice, LD vs pre/post: $p<0.001$ ). Saline injection did not significantly change SNr calcium signals (Figure S3.3E; N=8, saline vs pre/post:  $p=0.31/0.96$ ), nor did it increase movement velocity or significantly change rotation bias (Figure S3.3E). These findings support rate-model predictions, as well as prior experimental data, that dopamine replacement therapy inhibits basal ganglia output activity.

We then tested whether similar changes could be observed in the SNr during therapeutic STN DBS. As before, STN DBS increased movement velocity (Figure 3.2D-G, S3.3B-D). However, in contrast to levodopa, STN DBS (at both 60 and 100 Hz) *increased* SNr activity (Figure 3.2D-G, S3.3B-C; N=7 mice, stim vs pre/post:  $p<0.001$ ).

Thus, while both levodopa and STN DBS produced similar therapeutic increases in movement velocity, the two treatments evoked opposing changes in SNr activity.

### **STN DBS variably changes in hyperdirect M1 neural activity**

Another group of neurons which have been implicated in the therapeutic mechanisms of STN DBS is the hyperdirect pathway: primary motor cortex (M1) neurons that project monosynaptically to the STN. To assess changes in the activity of hyperdirect M1 neurons in response to levodopa and STN DBS, we used a retrograde viral strategy. We injected the STN of parkinsonian mice with one of two retrograde viruses encoding Cre recombinase (CAV2-Cre or rAAV2-Cre-mCherry), and injected M1 with Cre-dependent GCaMP6s. This strategy restricted expression of GCaMP6s to only STN-projecting M1 neurons. We then implanted an optical fiber in M1 and a DBS device in the STN (Figure 3.3A). We first administered levodopa, which increased movement velocity and rotational behavior (Figure 3.3B-C, S3.4A,D). During these sessions, hyperdirect M1 activity did not significantly change from baseline (Figure 3.3B-C; S3.4A; N=8, LD vs pre:  $p=0.078$ ). Injection with saline (N=8 mice) did not significantly alter movement parameters, nor change hyperdirect M1 activity (Figure S3.4E; saline vs pre/post:  $p=1.0/0.72$ ). These findings suggest that the behavioral effects of levodopa are not accompanied by significant modulation of hyperdirect M1 neurons.

As it has been suggested that antidromic activation of hyperdirect M1 neurons may play a role in the therapeutic response to STN DBS, we next examined whether STN DBS modulates hyperdirect M1 activity. As in other experiments, both 60 and 100 Hz stimulation consistently increased movement velocity (Figure 3.3D-E, S3.4B,D). During

60 Hz STN DBS, hyperdirect M1 calcium responses were surprisingly variable: just under half of the mice showed a decrease in hyperdirect M1 activity, and the rest showed either increases or no change (Figure 3.3D-E,H, S3.4B; stim vs pre/post:  $p=0.084/0.11$ ). In the same mice, 100 Hz stimulation produced similar increases in movement velocity, but evoked more consistent increases in M1 activity (Figure 3.3F-H, S3.4C;  $N=8$ , stim vs pre/post:  $p<0.001$ ). Given this seeming lack of correlation between hyperdirect M1 activity and the behavioral benefits of STN DBS, we wondered if the movement velocity of a single mouse during 60 Hz STN DBS could be predicted by whether that mouse showed increased or decreased M1 activity. Interestingly, movement velocity during stimulation was uncorrelated with the directionality of neural activity in M1 ( $R^2=-0.14$ ,  $p=0.96$ ). These findings suggest that while certain stimulation parameters may engage hyperdirect pathway activity, these changes do not correlate strongly with behavioral improvements during DBS.

**During STN DBS, changes in hyperdirect M1 activity occur much more slowly than changes in either STN activity, SNr activity, or movement velocity**

While only one of the three regions we recorded from showed significant responses to levodopa, all three regions showed significant changes to STN DBS for at least one stimulation frequency. Neurons that represent strong candidates in mediating the therapeutic effects of STN DBS would be predicted to show changes in activity on the timescale of behavioral benefits. In order to further explore how changes in neural activity correspond to changes in movement velocity, we measured the rise time of the calcium signal obtained in those brain regions and conditions in which we observed significant

changes in neural activity: STN (60 and 100 Hz), SNr (60 and 100 Hz), M1 hyperdirect (100 Hz). Given the observed lag between electrophysiology and bulk GCaMP signals<sup>22</sup>, we would expect that even changes in neural activity that drive behavior might appear to lag the behavior itself. Across all STN DBS conditions, the rise time for movement velocity averaged  $2.84 \pm 0.57$  sec. For each condition, we calculated the difference in rise time for the calcium signal and movement velocity, as an indicator of whether these two signals changed on a similar timescale. The rise time of STN calcium signals during 60 Hz or 100 Hz STN DBS lagged velocity rise time by  $2.56 \pm 1.14$  sec (Figure S3.2B-C). We observed a similarly short lag comparing SNr calcium signals to the corresponding movement velocity traces ( $3.71 \pm 1.77$  sec; S3B-C). However, the lag in hyperdirect M1 activity was markedly longer ( $17.25 \pm 3.05$  sec; S4B-C). Comparing these kinetics, changes in STN and SNr activity are stronger candidates than M1 hyperdirect activity in contributing to the therapeutic effects of STN DBS.

### **Optogenetic inhibition of SNr neurons or optogenetic activation of STN neurons increases movement in parkinsonian mice**

Contrary to rate-based predictions regarding changes in neural activity in response to antiparkinsonian treatments, we observed distinct, and sometimes opposing, changes in neural activity in response to levodopa and STN DBS. Treatments may evoke some changes in neural activity that drive motor improvement, while others changes may be correlated but not causal. To address this potential difference, we next tested whether manipulating neural activity, in the absence of levodopa or STN DBS, might be sufficient to improve movement velocity. The most salient effect of levodopa was to suppress SNr

activity. To simulate this effect, we injected parkinsonian VGAT-Cre mice with Cre-dependent halorhodopsin or eYFP (control) in the SNr (Figure 3.4A). To validate halorhodopsin function in SNr neurons, we performed cell-attached recordings in *ex vivo* slices (Figure 3.4B; n=17 cells, N=3 mice). As *in vivo*, SNr neurons fired spontaneously (Figure 3.4C). In response to one-minute periods of green light (6 mW), SNr neurons showed a significant decrease in firing rate (Figure 3.4C-D, S3.5A; stim vs pre/post:  $p < 0.001$ ). We then assessed motor behavior in response to one-minute epochs of green light (6 mW) *in vivo*. Optical inhibition of SNr activity increased movement velocity (Figure 3.4E-F, S3.5B; N=10; stim vs pre/post:  $p < 0.001$ ) and contralesional rotations (Figure 3.4G; stim vs pre/post:  $p < 0.001$ ), mimicking behavioral effects of levodopa administration. No change was seen in the behavior of eYFP-expressing mice in response to green light (Figure S3.5E; N=7 mice, stim vs pre/post:  $p = 0.98/0.93$ ). This result suggests that decreasing SNr activity is sufficient to increase movement in parkinsonian mice, and moreover may be a therapeutic mechanism of levodopa.

The most prominent effect of STN DBS in our experiments was an increase in STN calcium signals. To test whether this increase in STN activity was sufficient to produce therapeutic effects in parkinsonian mice, we injected VGlut2-Cre mice with Cre-dependent channelrhodopsin or eYFP (control) in the STN (Figure 3.4H). To validate the effects of channelrhodopsin on STN neural activity, we performed cell-attached recordings in *ex vivo* slices (Figure 3.4I; n=13 cells, N=3 mice). As *in vivo*, STN neurons fired spontaneously (Figure 3.4J). As predicted, STN neurons showed a significant increase in firing rate in response to one-minute epochs of pulsatile blue light stimulation

(Figure 3.4J-K; 50 Hz, 3 mW; stim vs pre/post:  $p < 0.05$ ), though the firing rate waned over the course of stimulation (Figure S3.5C). We then assessed the behavioral effects of pulsatile blue light stimulation (50 Hz, 3 mW) *in vivo*. Similar to electrical STN DBS, blue light stimulation increased movement velocity (Figure 3.4L-M, S5D; N=8, stim vs pre/post:  $p < 0.001$ ), but did not evoke a contralesional rotation bias (Figure 3.4N). Interestingly, movement velocity tended to peak early during stimulation, and fall off to a lower level (Figure S3.5D), similar to the firing rate decline observed during cell-attached recordings. Mice expressing eYFP (N=9 mice) did not show a significant change in movement velocity during blue light stimulation (Figure S3.5F; stim vs pre/post:  $p = 0.81/0.82$ ). Taken together, these results indicate that both inhibition of the SNr and excitation of the STN increase movement velocity in parkinsonian mice. Therefore, the seemingly paradoxical, opposing changes in activity evoked by levodopa and electrical STN DBS may in fact both contribute to the therapeutic effects on motor behavior.

## **Discussion**

We combined a recently developed mouse model of electrical STN DBS for Parkinson's disease<sup>20</sup> with electrical artifact-free GCaMP fiber photometry to compare the effects of levodopa and STN DBS on neural activity. While both levodopa and STN DBS similarly relieved bradykinesia, they had distinct, and in some cases opposing, effects on basal ganglia neural activity. Furthermore, optical manipulations that mimicked the effects of levodopa and STN DBS on neural activity both relieved bradykinesia, despite driving it in opposite directions.

In this study, we used calcium imaging with GCaMP6s to examine how neural activity changes during treatment with levodopa and STN DBS. To our knowledge, this is



one of the first studies to use calcium imaging with electrical STN DBS *in vivo* in parkinsonian animals. This approach had several advantages, as well as limitations. The key advantage was the ability to obtain recordings free from electrical artifacts. This had been a major obstacle in prior electrophysiological studies, particularly in studying the effect of DBS on the neurons in the target structure, such as the STN or GPi. A second advantage was the ability to use cell type- or projection-specific techniques in targeting neurons for imaging. For example, the use of retrograde viruses allowed us to target the direct projections from primary motor cortex to STN (hyperdirect pathway), a population of significant interest in PD and DBS. Though STN and SNr are relatively homogeneous structures, with regard to major neurotransmitters<sup>23,24</sup>, future studies could use GCaMP and genetics to target either specific STN/SNr projections, or novel cell types within them<sup>25,26</sup>. A disadvantage of our approach over traditional electrophysiology, however, is its temporal resolution. While extracellular electrophysiology can detect individual action potentials, calcium imaging with GCaMP likely integrates calcium over multiple spikes<sup>27</sup>. Fiber photometry further averages across a population of neurons, making it hard to detect rapid events or patterned activity. Nonetheless, given that our assessments of neural activity with photometry match those obtained with single-unit electrophysiology during levodopa treatment, there appears to be correspondence between the two recording techniques. In the future, voltage indicators with high signal-to-noise that are compatible with deep imaging, as well as miniscope imaging of many single neurons simultaneously, might allow detection of single spikes and help increase the information obtained in optical recordings during DBS.

On the whole, our reported effects of levodopa on neural activity support traditional models of basal ganglia function. We observed significant decreases in SNr activity in parallel with the therapeutic effects of levodopa, as has been seen in previous electrophysiological studies in humans, NHPs, and rats<sup>6,7,28</sup>. Interestingly, we did not see consistent changes in STN or M1 hyperdirect activity in response to levodopa, though we cannot rule out small changes that could not be detected with our methods or our sample size. The STN result does not conform to predictions of the rate model, but is consistent with the variety of responses reported in previous studies<sup>8-10</sup>. Little in the literature suggests how levodopa might impact hyperdirect M1 neurons.

However, our observation that therapeutic STN DBS *increased* activity at the level of the STN and SNr is at odds with rate-based models of basal ganglia function. Additionally, our data conflicts with some previous electrophysiological studies in primates<sup>14,15</sup>, but corresponds well to other studies<sup>16,17,29</sup>. Some discrepancies in existing physiological data may arise from electrical artifact removal from electrophysiological recordings, especially in structures like STN and SNr that have high spontaneous firing rates. Other discrepancies may relate to differences among animal models of PD.

Though we observed modulation of hyperdirect M1 neurons during STN DBS, this modulation did not correlate well with therapeutic effects. This disconnect has a number of potential explanations. Importantly, while past mouse studies have used optogenetic stimulation as a proxy for electrical STN DBS<sup>18,19</sup>, we used electrical stimulation in an effort to more closely model what is observed in PD patients. The former approach identifies manipulations which are sufficient to relieve parkinsonian motor symptoms,

while the latter identifies changes that correlate with a specific therapy. Thus, while optogenetic stimulation may reveal that changing neural activity in a variety of ways can relieve parkinsonism in mice, it is difficult to extrapolate which of these changes actually occur during electrical STN DBS. For instance, though our optogenetic experiments show that both inhibition of the SNr and excitation of the STN are therapeutic in parkinsonian mice, we only observe STN excitation during electrical STN DBS. In agreement with our findings in hyperdirect M1 neurons, a recent NHP study found that while some cortical neurons do show antidromic activation during STN DBS, cortical changes are inconsistent between animals and do not match the timescale of behavioral change<sup>30</sup>.

We found that therapeutic interventions produced both decreases (levodopa) or increases (STN DBS) in STN and/or SNr activity, and moreover that reproducing these changes with optical methods could also relieve parkinsonian motor deficits. These findings are at odds with the classical model of basal ganglia function, but are not without precedent. Indeed, recent chemogenetic and optogenetic studies indicate that activating *or* inhibiting STN neurons can relieve motor symptoms in parkinsonian mice<sup>31–33</sup>. Why might rate changes in either direction produce therapeutic effects? One possible explanation is that rate-independent aspects of neural activity, such as within-neuron firing pattern or between-neuron synchronization, may drive PD symptoms and represent key markers of therapeutic interventions, as has been postulated previously<sup>34–36</sup>. Many other groups have observed increased oscillations throughout the basal ganglia in parkinsonian animal models and in humans, which may resolve with therapeutic treatment<sup>37–40</sup>. If this is the case, though levodopa and STN DBS may drive opposing

changes in firing rate, they may both interrupt the pathological rhythmicity observed in PD. This possibility might be investigated in the future using a combination of optical and electrical methods, building on the approach introduced here.

Excitingly, our observation that bidirectional changes in basal ganglia activity confer therapeutic benefit in a mouse model of PD suggests a wider therapeutic space for the treatment of PD. Most therapeutic approaches to PD have been predicated on the idea that inhibition of hyperactive basal ganglia nuclei is required for therapeutic benefit, but we now know that both increases and decreases in activity can improve movement. In addition, our work linking neural activity to behavior in STN DBS for PD may inform the application of DBS to other neuropsychiatric disorders. To rationally apply DBS to other conditions, such as addiction or Tourette's syndrome, it is critical to know how electrical stimulation might impact the underlying neural circuitry of disease.

## **Methods**

### **Animals**

3-6-month-old wild-type and transgenic C57Bl/6 mice of either sex were used in this study. To allow optical recording and manipulation of glutamatergic STN neurons, homozygous VGlut2-Cre mice (Stock No. 028863, Jackson Labs) were bred to wild-type C57Bl/6 mice (Jackson Labs) to yield hemizygous VGlut2-Cre mice. To allow optical recording and manipulation of GABAergic SNr neurons, homozygous VGAT-Cre mice (Jackson Labs) were bred to wild-type C57Bl/6 mice (Jackson Labs) to yield hemizygous VGAT-Cre mice. Animals were housed 1-5 per cage on a 12-hour light/dark cycle with *ad libitum* access to rodent chow and water. All behavioral manipulations were performed during the light phase. We complied with local and national ethical regulations regarding the use of mice in research. All experimental protocols were approved by the UC San Francisco Institutional Animal Care and Use Committee.

### **Surgical Procedures**

Stereotaxic surgery was performed between 3 and 6 months of age. Anesthesia was induced with intraperitoneal (IP) injection (0.1 mL) of ketamine (40 mg/kg) and xylazine (10 mg/kg) and maintained with inhaled isoflurane (0.5%-1%). To model Parkinson's disease in mice, the neurotoxin 6-hydroxydopamine (6-OHDA, 1  $\mu$ L, 5 mg/mL) was injected unilaterally in the left medial forebrain bundle (MFB, -1.0 AP, -1.0 ML, 4.9 DV). Desipramine (0.2 mL, 2.5 mg/mL) was injected intraperitoneally (IP) approximately 30 min prior to 6-OHDA injections to reduce uptake by other monoaminergic neurons in the MFB. Additional surgeries were performed at least two weeks following MFB injection.

For experiments involving electrical STN DBS, a 3-lead bipolar stimulating electrode array was implanted in the ipsilesional STN (-1.8 AP, -1.65 ML, 4.5 DV) <sup>20</sup>. During the same surgery, VGlut2-Cre mice were injected with Cre-dependent AAV1-Syn-Flex-GCaMP6s-WPRE-SV40 (UPenn, 100 nL) in the STN (-1.8 AP, -1.65 ML, 4.5 DV) and implanted with a photometry fiber-optic ferrule (0.4 mm, Doric Lenses) above the STN (4.3 DV). VGAT-Cre mice were injected with the Cre-dependent GCaMP6s vector (300-500 nL) in the SNr (-3.2 AP, -1.6 ML, 4.5 DV) and implanted with a fiber-optic ferrule above the SNr (4.3 DV). Wild-type mice were injected with a retrograde virus encoding Cre recombinase [either CAV-Cre (Montpellier, 100 nL) or AAV2<sub>retro</sub>-Cre-mCherry (Addgene/UPenn Vector Core, 100 nL)] in the STN (-1.8 AP, -1.65 ML, 4.5 DV) and Cre-dependent GCaMP6s (500 nL) in the primary motor cortex (M1, +2 AP, -1.56 ML, 1 DV) and implanted with a fiber-optic ferrule above M1 (0.8 DV).

For optical stimulation experiments, VGlut2-Cre mice were injected with Cre-dependent AAV5-DIO-ChR2-eYFP (UPenn, diluted 1:2 in normal saline, 100 nL) or AAV5-DIO-eYFP (UNC, 100 nL) and implanted with a fiber-optic ferrule (0.2 mm, Thor Labs) above the STN (4.3 DV). VGAT-Cre mice were injected with Cre-dependent AAV5-DIO-eNpHR3.0-eYFP (UNC Vector Core, 300 nL) or AAV5-DIO-eYFP (UNC, 300 nL) and implanted with a fiber-optic ferrule (0.2 mm, Thor Labs) above the SNr (4.3 DV).

A minimum of 3 weeks of viral expression was allowed before behavioral testing.

## **Behavior**

All behavior was conducted in the open field (clear acrylic cylinders, 25 cm diameter) following 1 day of habituation (20 minutes). Mice were monitored via two cameras, one directly above and one in front of the chamber. Video-tracking software (Noldus Ethovision) was used to quantify locomotor activity, including movement velocity, ipsilateral rotations, and contralateral rotations. Dyskinesia was scored manually by an unblinded rater using a modified version of the abnormal involuntary movements (AIM) scoring method <sup>21</sup>. Dyskinesia was quantified in one-minute increments either every minute (for STN DBS experiments) or every 5 minutes (for levodopa experiments), with axial, limb, and orofacial body segments rated on a scale of 0-3 each. A score of 0 indicates no abnormal movement, while a score of 3 indicates continuous dyskinesia for the one minute epoch. The scores for each body segment are then summed, with a maximum score of 9 per epoch.

## **Pharmacology**

6-OHDA (Sigma Aldrich) was prepared at 5 mg/mL in normal saline. Levodopa was prepared (0.5 mg/mL Sigma Aldrich) with benserazide (0.25 mg/mL, Sigma Aldrich) in normal saline and always administered at 5 mg/kg.

## **Electrical Stimulation**

An isolated constant current bipolar stimulator (WPI) was used to deliver electrical stimuli. The timing of stimuli was controlled by TTL input from an Arduino. Electrical stimulation experiments consisted of five 1 min stimulation periods, each preceded and followed by

1 min of no stimulation, for a total of 11 min. Both the construction of STN DBS electrodes and the determination of optimal stimulation electrode pair were as detailed previously<sup>20</sup>.

### **Fiber Photometry**

Fiber photometry signals were acquired through implanted 400  $\mu\text{m}$  optical fibers, using an LED driver system (Doric). Following signal modulation, 405 nm (control signal, from GCaMP autofluorescence) and 465 nm signals were demodulated via a lock-in amplifier (RZ5P, TDT), visualized, and recorded (Synapse, TDT). Offline, the 405 nm signal was fit to the 465 nm signal using a first-degree polynomial fit (Matlab) to extract the non-calcium dependent signal (due to autofluorescence, fiber bending, etc). This was then subtracted from the 465 nm signal to generate a motion-corrected signal. To remove the gradual, slow bleaching observed in the  $\sim$ 3 hour saline and levodopa recordings, we additionally fit a double exponential to the 405 nm signal, linearly fit it to the motion-corrected signal, and then subtracted it.

Every processed fiber photometry signal was normalized (z-scored) by subtracting the mean and dividing by the standard deviation of the closest preceding “pre” period. For electrical stimulation experiments, the 30 seconds preceding each stimulation period was used to normalize the subsequent 1-min stim and 1-min post period. For levodopa and saline experiments, the 20 minutes prior to injection was used to normalize the subsequent 2.5 hours of signal.

### ***Ex vivo* Slice Electrophysiology and Imaging**

To prepare *ex vivo* slices for whole-cell recordings and GCaMP imaging, mice were deeply anesthetized with IP ketamine-xylazine, transcardially perfused with ice-cold



glycerol-based slicing solution, decapitated, and the brain was removed. Glycerol-based slicing solution contained (in mM): 250 glycerol, 2.5 KCl, 1.2 NaH<sub>2</sub>PO<sub>4</sub>, 10 HEPES, 21 NaHCO<sub>3</sub>, 5 glucose, 2 MgCl<sub>2</sub>, 2 CaCl<sub>2</sub>. The brain was mounted on a submerged chuck, and sequential 275 μm coronal or sagittal slices were cut on a vibrating microtome (Leica), transferred to a chamber of warm (34°C) carbogenated ACSF containing (in mM) 125 NaCl, 26 NaHCO<sub>3</sub>, 2.5 KCl, 1 MgCl<sub>2</sub>, 2 CaCl<sub>2</sub>, 1.25 NaH<sub>2</sub>PO<sub>4</sub>, 12.5 glucose for 30-60 min, then stored in carbogenated ACSF at room temperature. Each slice was then submerged in a chamber superfused with carbogenated ACSF at 31°C-33°C for recordings. STN or SNr neurons were targeted using differential interference contrast (DIC) optics in VGlut2-Cre or VGAT-Cre mice, respectively, on an Olympus BX 51 WIF microscope.

For opsin validation experiments, neurons were patched in the cell-attached configuration using borosilicate glass electrodes (3-5 MΩ) filled with ACSF. Picrotoxin was added to all external solutions for opsin validation. For combined electrophysiology-imaging experiments with GCaMP6s, neurons were patched in the whole-cell current-clamp configuration using borosilicate glass electrodes (3-5 MΩ) filled with potassium methanesulfonate-based internal solution containing (in mM): 130 KMeSO<sub>3</sub>, 10 NaCl, 2 MgCl<sub>2</sub>, 0.16 CaCl<sub>2</sub>, 0.5 EGTA, 10 HEPES, 2 MgATP, 0.3 NaGTP, pH 7.3. All recordings were made using a MultiClamp 700B amplifier (Molecular Devices) and digitized with an ITC-18 A/D board (HEKA). Data were acquired using Igor Pro 6.0 software (Wavemetrics) and custom acquisition routines (mafPC, courtesy of M. A. Xu-Friedman). Recordings were filtered at 5 kHz and digitized at 10 kHz.

To validate ChR2 or eNpHR3.0 function in slice, light pulses were delivered to the slice by a TTL-controlled LED (Olympus), passed through a GFP (473 nm) or TxRed (562 nm) filter (Chroma) and the 40X immersion objective. LED intensity was adjusted to yield an output of either 3 mW (for ChR2) or 6 mW (for eNpHR3.0) at the slice. Light was delivered in 1 minute epochs, at 50 Hz, 3 ms pulse width (for ChR2) or continuously (for eNpHR3.0). Stimulation lasted for 1 min and was preceded and followed by 30 seconds of recording without stimulation.

For simultaneous electrophysiology and GCaMP6s imaging, current-clamped neurons were stimulated (0.5-1 nA) to elicit action potentials. Stimulation occurred at 10 Hz; 50 or 60 Hz; 100 or 120 Hz (100  $\mu$ s pulse-width); or was delivered as a long single square wave of constant current for 1 min, preceded and followed by 30 seconds without stimulation. During the duration of each 2 min trial GCaMP fluorescence was either acquired through 1-photon or 2-photon microscopy. 1-photon experiments used a 473 nm light (TTL-controlled LED, Olympus, paired with GFP filter, Chroma) delivered to the slice at <1 mW, with GCaMP6s fluorescence captured using an imaging camera attached to the microscope (QI Retiga Electro). For 2-photon microscopy, a 2-photon source (Coherent Ultra II) was tuned to 810 nm to identify GCaMP expressing neurons, and tuned to 940 nm for calcium imaging. Epi- and transfluorescence signals were captured through a 40 $\times$ , 0.8 NA objective paired with a 1.4 NA oil immersion condenser (Olympus) to photomultiplier tubes (H10770PA-40 PMTs, Hamamatsu). Data were collected in line scan mode (2–2.4 ms/line, including mirror flyback).

All *ex vivo* electrical recordings were passed through a 1 Hz high-pass filter to remove slow electrical drift and spikes were extracted using the findpeaks function in

Matlab. All *ex vivo* optical recordings were first collapsed into a one-dimensional fluorescence time series by averaging the fluorescence of pixels within a defined region-of-interest. In one-photon recordings, this signal was further processed by fitting a double exponential and subtracting it to remove effects of signal bleaching.

### **Optogenetic Manipulations**

Prior to optical stimulation experiments, animals were habituated to tethering with custom lightweight patch cables (Precision Fiber Products and ThorLabs) coupled to an optical commutator (Doric Lenses) in the open field for 30 min per day, over 1-2 days. Optical stimulation sessions consisted of five 1 min stimulation periods, each preceded and followed by 1 min of no stimulation, for a total of 11 min. TTL-controlled (Master8, A.M.P.I.) blue (488 nm, 3 mW, Shanghai Laser and Optics Century) or green laser light (593 nm, 6 mW, Shanghai Laser and Optics Century) was delivered in pulse trains (3 ms, 50Hz) or continuously, respectively.

### **Histology and Microscopy**

Mice were terminally anesthetized with IP ketamine (200 mg/kg) and xylazine (40 mg/kg). For mice with an implanted STN DBS device, the site of stimulation was marked with a solid state, direct current Lesion Maker (Ugo Basile). Mice were then transcardially perfused with 4% paraformaldehyde (PFA), the brain was dissected from the skull and fixed overnight in 4% PFA, and then was placed in 30% sucrose at 4°C for 2-3 days. Brains were then cut into 50  $\mu$ m sagittal sections on a freezing microtome (Leica). To confirm dopamine depletion, tissue was immunostained for tyrosine hydroxylase (TH). Stitched multi-channel fluorescence images were taken on a Nikon 6D conventional widefield

microscope at 4-10X, using custom software (UCSF Nikon Imaging Center) to confirm virus expression, fiber placement, and STN DBS placement on a subset of animals.

### **Quantification and Statistical Analysis**

All data are expressed as mean  $\pm$  standard error of the mean (SEM). For all bar graphs for electrical stimulation, optogenetic, and slice experiments, the “stim” bar was calculated by averaging all one-minute stimulation periods for each trial. The “pre” and “post” bars were calculated by averaging the 30 seconds before and 30 seconds after each stimulation period, respectively. For all bar graphs involving levodopa or saline, the “LD” or “saline” bar was calculated by averaging the ten minutes between 30-40 min post injection for each trial. The “pre” and “post” bars were calculated by averaging the ten minutes 15-5 min before injection and 125-135 min post injection, respectively, for each trial. Rise time of velocity and calcium signals was calculated as the time it took from the onset of stimulation for the signal to first reach the mean value for that stimulation epoch.

All data was tested for normality using a Kolmogorov-Smirnov (KS) test. A Friedman test was used for data that did not pass the KS test (Supplementary Fig 3.1D,H-I,M-N), and a one-way repeated measures ANOVA was used for data that did (all other figures). In both cases, a Tukey HSD post hoc analysis was applied to correct for multiple comparisons. Data was considered statistically significant for  $p < 0.05$ .

### **Contributions**

JSS, ABN, and KJB designed the experiments. JSS, IGM, PWES, and RJB performed experiments. JSS and ABN wrote the manuscript with contributions from all authors.

## **Acknowledgements**

The authors would like to acknowledge P. Starr, J. Ostrem, G. Bouvier, and members of the Nelson Lab and Bender Lab for providing advice and feedback on the manuscript.

This work was supported by the NINDS (K08 NS081001, ABN; F31 NS110329, JSS) and the UCSF Discovery Fellows Program (JSS). ABN is the Richard and Shirley Cahill Endowed Chair in Parkinson's Disease Research.

## References

1. Albin, R. L., Young, A. B. & Penney, J. B. The functional anatomy of basal ganglia disorders. *Trends Neurosci.* **12**, 366–375 (1989).
2. DeLong, M. R. Primate models of movement disorders of basal ganglia origin. *Trends Neurosci.* **13**, 281–285 (1990).
3. Rubin, J. E., McIntyre, C. C., Turner, R. S. & Wichmann, T. Basal ganglia activity patterns in parkinsonism and computational modeling of their downstream effects. *Eur. J. Neurosci.* **36**, 2213–2228 (2012).
4. Hutchinson, W. D., Levy, R., Dostrovsky, J. O., Lozano, A. M. & Lang, A. E. Effects of apomorphine on globus pallidus neurons in parkinsonian patients. *Ann. Neurol.* **42**, 767–775 (1997).
5. Lozano, A. M., Lang, A. E., Levy, R., Hutchison, W. & Dostrovsky, J. Neuronal recordings in Parkinson's disease patients with dyskinesias induced by apomorphine. *Ann. Neurol.* **47**, S141-146 (2000).
6. Meissner, W. *et al.* Increased slow oscillatory activity in substantia nigra pars reticulata triggers abnormal involuntary movements in the 6-OHDA-lesioned rat in the presence of excessive extracellular striatal dopamine. *Neurobiol. Dis.* **22**, 586–598 (2006).
7. Papa, S. M., Desimone, R., Fiorani, M. & Oldfield, E. H. Internal globus pallidus discharge is nearly suppressed during levodopa-induced dyskinesias. *Ann. Neurol.* **46**, 732–738 (1999).

8. Tachibana, Y., Iwamuro, H., Kita, H., Takada, M. & Nambu, A. Subthalamo-pallidal interactions underlying parkinsonian neuronal oscillations in the primate basal ganglia. *Eur. J. Neurosci.* **34**, 1470–1484 (2011).
9. Kreiss, D. S., Mastropietro, C. W., Rawji, S. S. & Walters, J. R. The response of subthalamic nucleus neurons to dopamine receptor stimulation in a rodent model of Parkinson's disease. *J. Neurosci. Off. J. Soc. Neurosci.* **17**, 6807–6819 (1997).
10. Levy, R. *et al.* Effects of apomorphine on subthalamic nucleus and globus pallidus internus neurons in patients with Parkinson's disease. *J. Neurophysiol.* **86**, 249–260 (2001).
11. Andy, O. J., Jurko, M. F. & Sias, F. R. Subthalamotomy in Treatment of Parkinsonian Tremor. *J. Neurosurg.* **20**, 860–870 (1963).
12. Bergman, H., Wichmann, T. & DeLong, M. R. Reversal of experimental parkinsonism by lesions of the subthalamic nucleus. *Science* **249**, 1436–1438 (1990).
13. Chiken, S. & Nambu, A. Disrupting neuronal transmission: mechanism of DBS? *Front. Syst. Neurosci.* **8**, (2014).
14. Filali, M., Hutchison, W. D., Palter, V. N., Lozano, A. M. & Dostrovsky, J. O. Stimulation-induced inhibition of neuronal firing in human subthalamic nucleus. *Exp. Brain Res.* **156**, 274–281 (2004).

15. Moran, A., Stein, E., Tischler, H., Belevsky, K. & Bar-Gad, I. Dynamic Stereotypic Responses of Basal Ganglia Neurons to Subthalamic Nucleus High-Frequency Stimulation in the Parkinsonian Primate. *Front. Syst. Neurosci.* **5**, (2011).
16. Hashimoto, T., Elder, C. M., Okun, M. S., Patrick, S. K. & Vitek, J. L. Stimulation of the subthalamic nucleus changes the firing pattern of pallidal neurons. *J. Neurosci.* **23**, 1916–1923 (2003).
17. Reese, R. *et al.* Subthalamic deep brain stimulation increases pallidal firing rate and regularity. *Exp. Neurol.* **229**, 517–521 (2011).
18. Gradinaru, V., Mogri, M., Thompson, K. R., Henderson, J. M. & Deisseroth, K. Optical Deconstruction of Parkinsonian Neural Circuitry. *Science* **324**, 354–359 (2009).
19. Sanders, T. H. & Jaeger, D. Optogenetic stimulation of cortico-subthalamic projections is sufficient to ameliorate bradykinesia in 6-ohda lesioned mice. *Neurobiol. Dis.* **95**, 225–237 (2016).
20. Schor, J. S. & Nelson, A. B. Multiple stimulation parameters influence efficacy of deep brain stimulation in parkinsonian mice. *J. Clin. Invest.* **129**, 3833–3838 (2019).
21. Cenci, M. A. & Lundblad, M. Ratings of L-DOPA-induced dyskinesia in the unilateral 6-OHDA lesion model of Parkinson's disease in rats and mice. *Curr. Protoc. Neurosci.* **Chapter 9**, Unit 9.25 (2007).
22. Markowitz, J. E. *et al.* The Striatum Organizes 3D Behavior via Moment-to-Moment Action Selection. *Cell* **174**, 44-58.e17 (2018).



23. Smith, Y. & Parent, A. Neurons of the subthalamic nucleus in primates display glutamate but not GABA immunoreactivity. *Brain Res.* **453**, 353–356 (1988).
24. Walaas, I. & Fonnum, F. The distribution and origin of glutamate decarboxylase and choline acetyltransferase in ventral pallidum and other basal forebrain regions. *Brain Res.* **177**, 325–336 (1979).
25. Kita, H. & Kitai, S. T. Efferent projections of the subthalamic nucleus in the rat: light and electron microscopic analysis with the PHA-L method. *J. Comp. Neurol.* **260**, 435–452 (1987).
26. Liu, D. *et al.* A common hub for sleep and motor control in the substantia nigra. *Science* **367**, 440–445 (2020).
27. Chen, T.-W. *et al.* Ultra-sensitive fluorescent proteins for imaging neuronal activity. *Nature* **499**, 295–300 (2013).
28. Starr, P. A. *et al.* Spontaneous pallidal neuronal activity in human dystonia: comparison with Parkinson's disease and normal macaque. *J. Neurophysiol.* **93**, 3165–3176 (2005).
29. Zhao, S. *et al.* Full activation pattern mapping by simultaneous deep brain stimulation and fMRI with graphene fiber electrodes. *Nat. Commun.* **11**, 1788 (2020).
30. Johnson, L. A. *et al.* Direct Activation of Primary Motor Cortex during Subthalamic But Not Pallidal Deep Brain Stimulation. *J. Neurosci.* **40**, 2166–2177 (2020).

31. McIver, E. L. *et al.* Maladaptive Downregulation of Autonomous Subthalamic Nucleus Activity following the Loss of Midbrain Dopamine Neurons. *Cell Rep.* **28**, 992-1002.e4 (2019).
32. Yoon, H. H. *et al.* Optogenetic inactivation of the subthalamic nucleus improves forelimb akinesia in a rat model of Parkinson disease. *Neurosurgery* **74**, 533–540; discussion 540-541 (2014).
33. Yu, C., Cassar, I. R., Sambangi, J. & Grill, W. M. Frequency-Specific Optogenetic Deep Brain Stimulation of Subthalamic Nucleus Improves Parkinsonian Motor Behaviors. *J. Neurosci.* **40**, 4323–4334 (2020).
34. Hammond, C., Bergman, H. & Brown, P. Pathological synchronization in Parkinson's disease: networks, models and treatments. *Trends Neurosci.* **30**, 357–364 (2007).
35. Little, S. & Brown, P. The functional role of beta oscillations in Parkinson's disease. *Parkinsonism Relat. Disord.* **20 Suppl 1**, S44-48 (2014).
36. Wichmann, T. Changing views of the pathophysiology of Parkinsonism. *Mov. Disord. Off. J. Mov. Disord. Soc.* **34**, 1130–1143 (2019).
37. Halje, P. *et al.* Levodopa-Induced Dyskinesia Is Strongly Associated with Resonant Cortical Oscillations. *J. Neurosci.* **32**, 16541–16551 (2012).
38. de Hemptinne, C. *et al.* Therapeutic deep brain stimulation reduces cortical phase-amplitude coupling in Parkinson's disease. *Nat. Neurosci.* **18**, 779–786 (2015).

39. Moran, A., Stein, E., Tischler, H. & Bar-Gad, I. Decoupling neuronal oscillations during subthalamic nucleus stimulation in the parkinsonian primate. *Neurobiol. Dis.* **45**, 583–590 (2012).

40. Shimamoto, S. A. *et al.* Subthalamic nucleus neurons are synchronized to primary motor cortex local field potentials in Parkinson's disease. *J. Neurosci. Off. J. Soc. Neurosci.* **33**, 7220–7233 (2013).

**Figure 3.1**

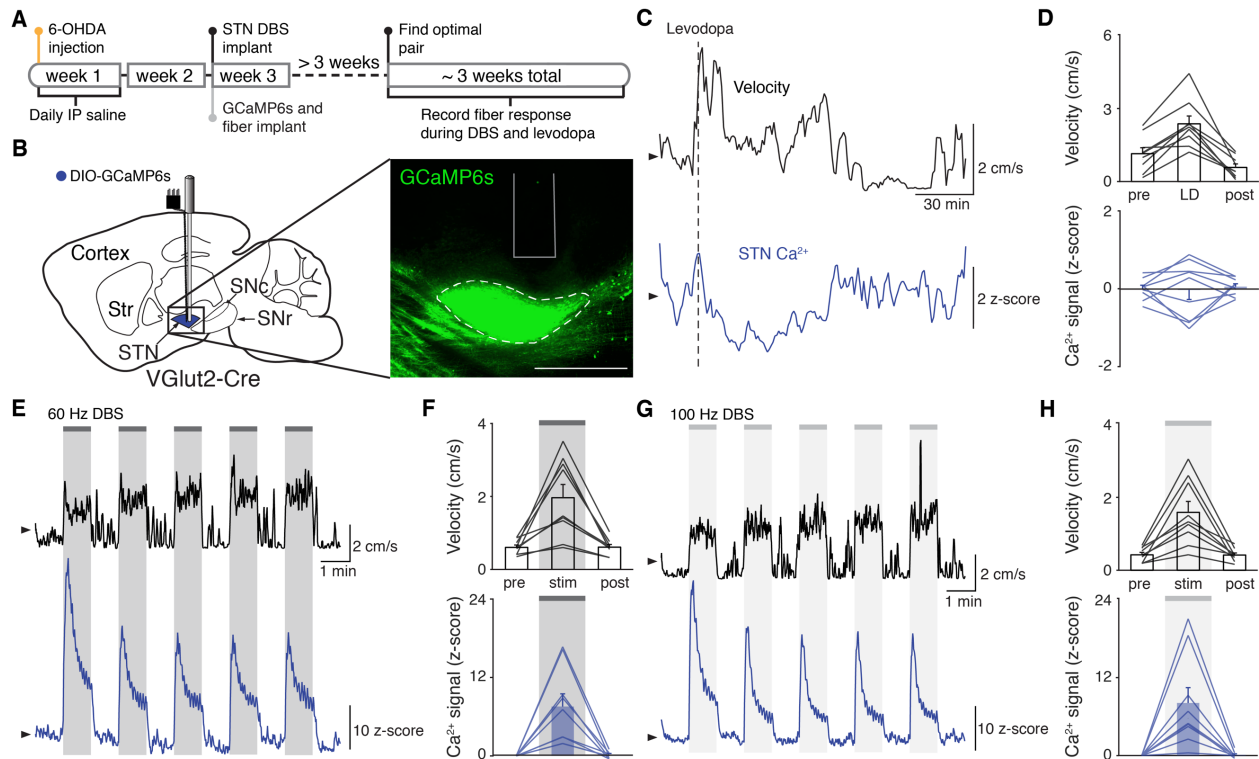


**Figure 3.1. Deep brain stimulation (DBS) of the subthalamic nucleus (STN) increases STN activity.** Hemiparkinsonian VGlut2-Cre mice were injected with Cre-dependent GCaMP6s and implanted with an electrical DBS device and optical fiber in the ipsilateral STN. **(A)** Experimental timeline. **(B)** Left: Sagittal schematic showing STN DBS and GCaMP fiber photometry. Right: Postmortem sagittal section showing GCaMP expression and estimated fiber placement in the STN (inset, scale=500  $\mu$ m). **(C)** Representative single-session velocity (black) and STN GCaMP signal (blue) before and after levodopa injection (dotted line). **(D)** Average velocity (top) and STN GCaMP signal (bottom) before, during, and after levodopa treatment. **(E)** Representative single-session velocity (black) and STN GCaMP signal (blue) in response to 60 Hz STN DBS. **(F)** Average velocity (top) and STN GCaMP signal (bottom) before, during, and after 60 Hz STN DBS. **(G)** Representative single-session velocity (black) and STN GCaMP signal (blue) in response to 100 Hz STN DBS. **(H)** Average velocity (top) and STN GCaMP signal (bottom) before, during, and after 100 Hz STN DBS. Arrowhead in velocity traces and GCaMP traces corresponds to 1 cm/s and 0 z-score, respectively. N=9 mice. Bar plots show mean  $\pm$  SEM.

**Figure 3.2**

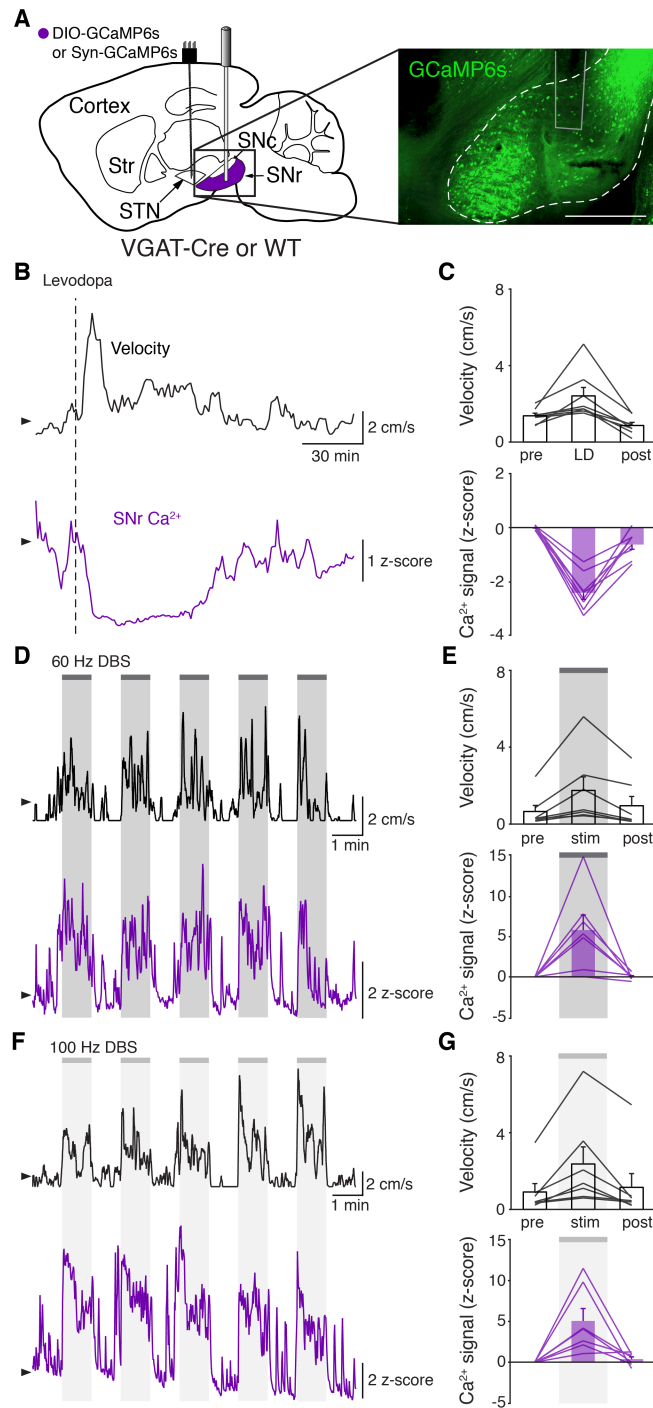


**Figure 3.2. STN DBS and levodopa have opposite effects on activity in the substantia nigra pars reticulata (SNr).** Hemiparkinsonian mice were injected with GCaMP6s in the SNr and implanted with an electrical DBS device in the STN and an optical fiber in the ipsilateral SNr. **(A)** Left: Sagittal schematic showing STN DBS and SNr GCaMP fiber photometry. Right: Postmortem sagittal section showing GCaMP

expression and estimated fiber placement in the SNr (inset, scale=500  $\mu$ m). **(B)** Representative single-session velocity (black) and SNr GCaMP signal (purple) before and after levodopa injection (dotted line). **(C)** Average velocity (top) and SNr GCaMP signal (bottom) before, during, and after levodopa treatment. **(D)** Representative single-session velocity (black) and SNr GCaMP signal (purple) in response to 60 Hz STN DBS. **(E)** Average velocity (top) and SNr GCaMP signal (bottom) before, during, and after 60 Hz STN DBS (N=7 mice). **(F)** Representative single-session velocity (black) and SNr GCaMP signal (purple) in response to 100 Hz STN DBS. **(G)** Average velocity (top) and SNr GCaMP signal (bottom) before, during, and after 100 Hz STN DBS (N=7 mice). Arrowhead in velocity traces and GCaMP traces corresponds to 1 cm/s and 0 z-score, respectively. N=7-8 mice. Bar plots show mean  $\pm$  SEM.

**Figure 3.3**

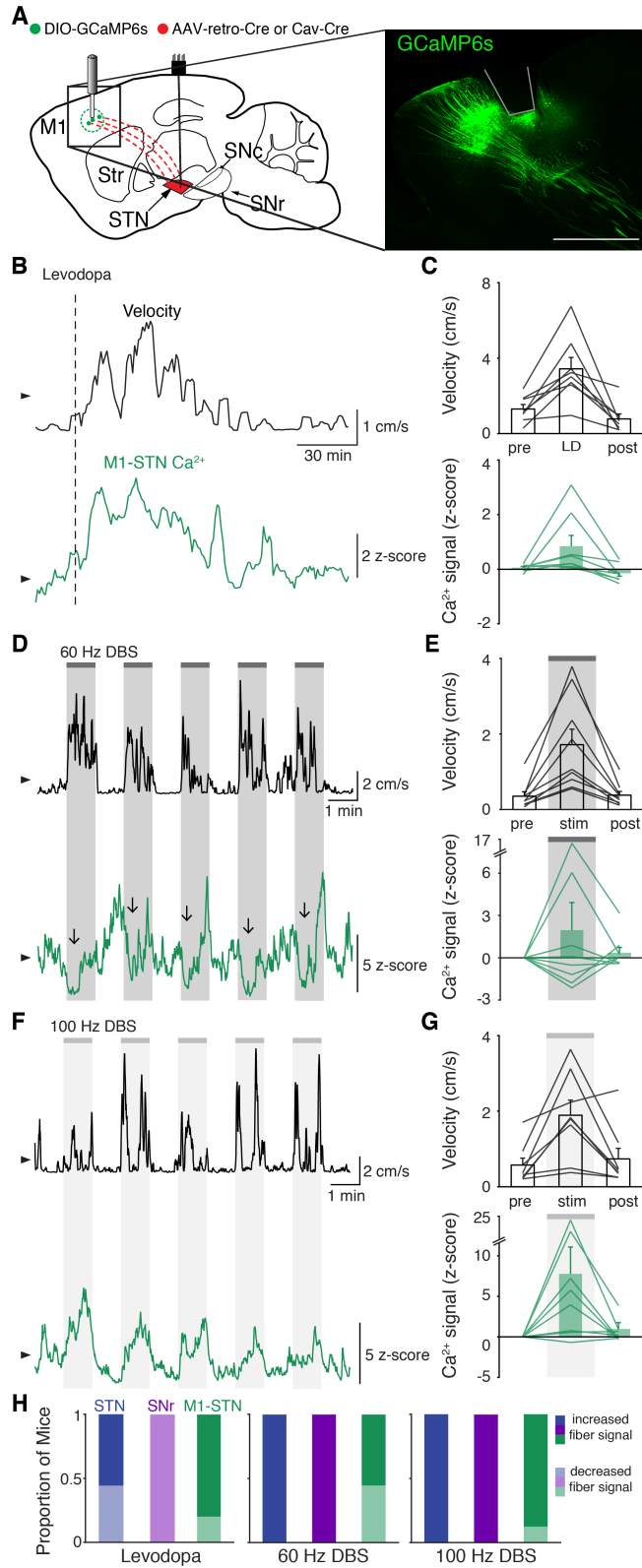


**Figure 3.3. The responses of hyperdirect primary motor cortex (M1) neurons to STN DBS do not consistently correlate with motor benefits.** To target hyperdirect pathway (STN-projecting M1) neurons, hemiparkinsonian mice were injected with a retrograde virus encoding Cre in the STN, and Cre-dependent GCaMP6s in the ipsilateral M1 cortex. **(A)** Left: Sagittal schematic showing STN DBS and M1-STN GCaMP fiber photometry. Right: Postmortem sagittal section showing GCaMP expression in M1 (inset, scale=500  $\mu$ m). **(B)** Representative single-session velocity (black) and M1-STN GCaMP signal (green) before and after levodopa injection (dotted line). **(C)** Average velocity (top) and M1-STN GCaMP signal (bottom) before, during, and after levodopa treatment. **(D)** Representative single-session velocity (black) and M1-STN GCaMP signal (green) in response to 60 Hz STN DBS. Vertical arrows indicate a decrease in GCaMP signal following stimulation onset. **(E)** Average velocity (top) and M1-STN GCaMP signal (bottom) before, during, and after 60 Hz STN DB. **(F)** Representative single-session velocity (black) and M1-STN GCaMP signal (green) in response to 100 Hz STN DBS. **(G)** Average velocity (top) and M1-STN GCaMP signal (bottom) before, during, and after 100 Hz STN DB. **(H)** Proportion of mice in which the indicated brain regions showed an increase or decrease in GCaMP signal during levodopa treatment (left), 60 Hz STN DBS (center), or 100 Hz STN DBS (right). Arrowhead in velocity traces and GCaMP traces corresponds to 1 cm/s and 0 z-score, respectively. N=8-9 mice. Bar plots show mean  $\pm$  SEM.



**Figure 3.4**

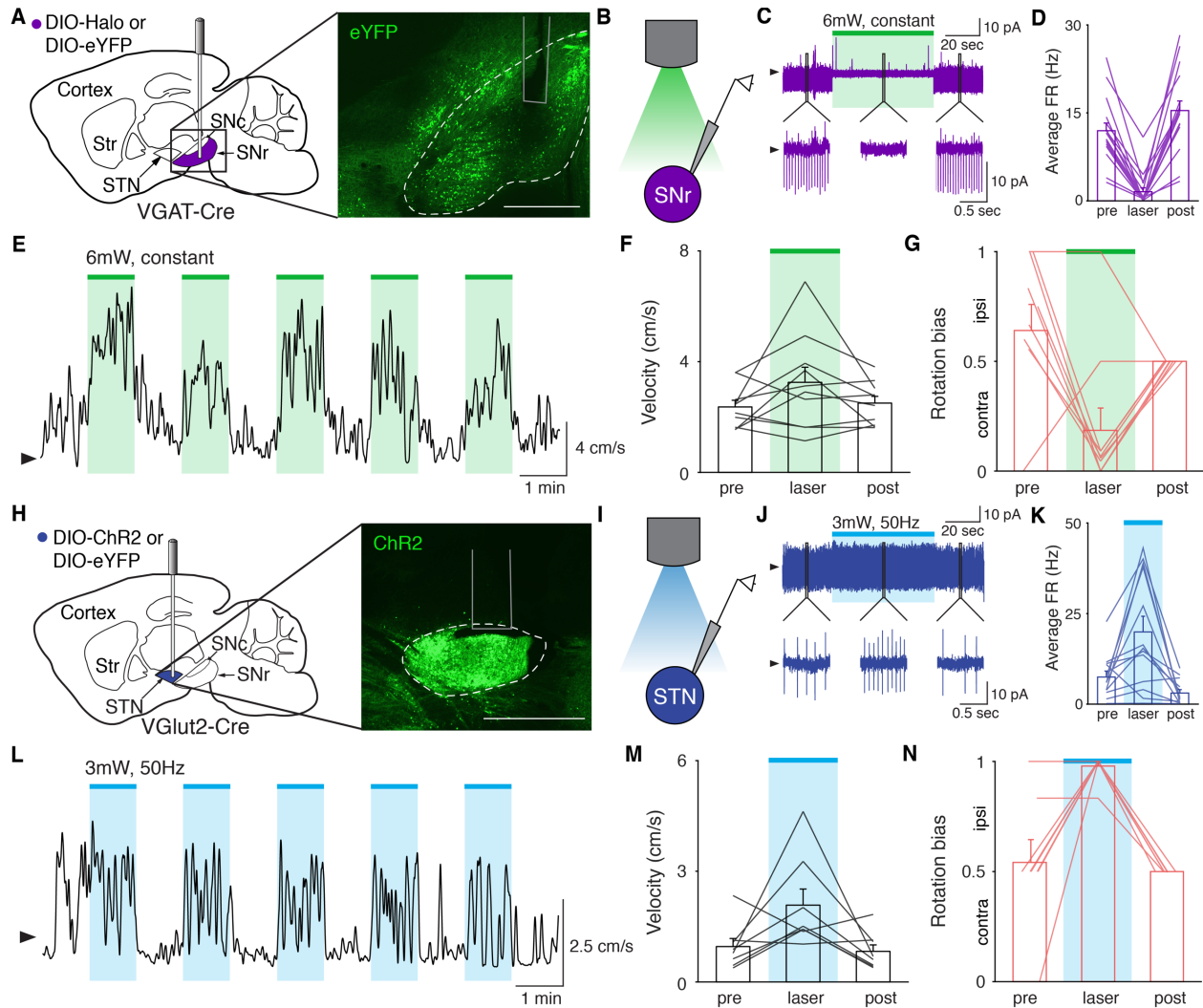
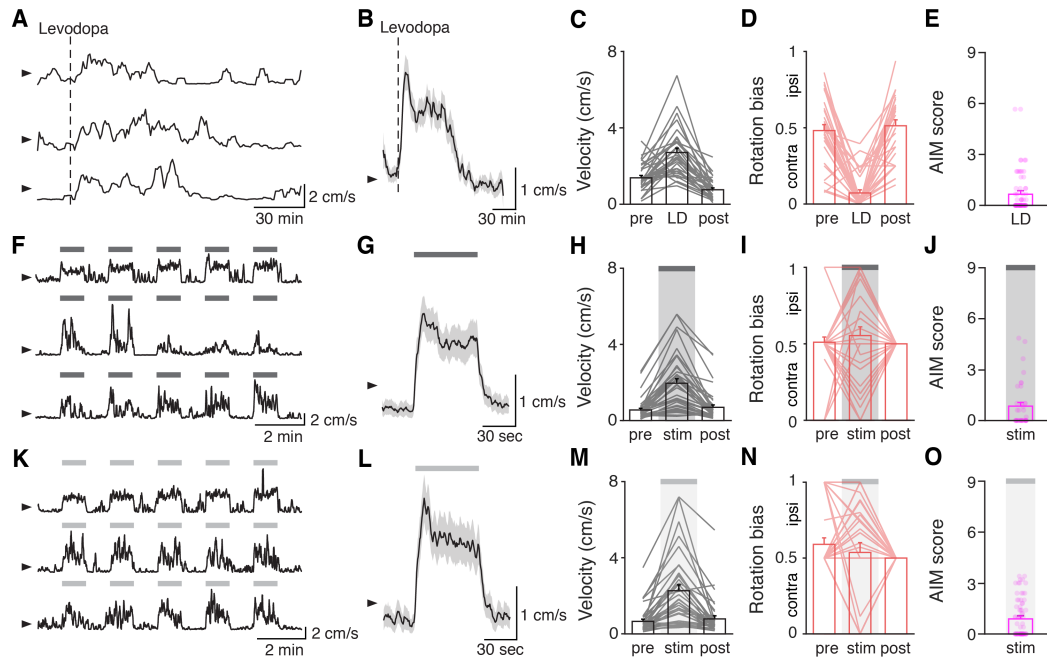


**Figure 3.4. Optogenetic inhibition of SNr and optogenetic excitation of STN increase movement in parkinsonian mice.** (A-G) Hemiparkinsonian VGAT-Cre mice were injected with Cre-dependent eNphR3.0 or eYFP, and implanted with an optical fiber in the ipsilateral SNr. **(A)** Left: Sagittal schematic showing viral injection and optical fiber implantation in the SNr. Right: Postmortem sagittal section showing eYFP expression in the SNr (inset, scale=500 $\mu$ m). **(B-D)** Ex vivo recordings of SNr neurons in the cell-attached configuration. **(B)** Recording configuration. **(C)** Representative SNr neuron before, during, and after green light stimulation (1 minute). 1 second portions of the sweep are shown below. **(D)** Average firing rate before, during, and after stimulation (n=17 cells, N=3 mice). **(E)** Representative single-session velocity in response to green light stimulation (1 minute). **(F)** Average velocity before, during, and after stimulation (N=10 mice). **(G)** Average rotation bias of parkinsonian mice before, during, and after stimulation (N=10 mice). (H-N) Hemiparkinsonian VGlut2-Cre mice were injected with Cre-dependent ChR2 or eYFP, and implanted with an optical fiber over the ipsilateral STN. **(H)** Left:

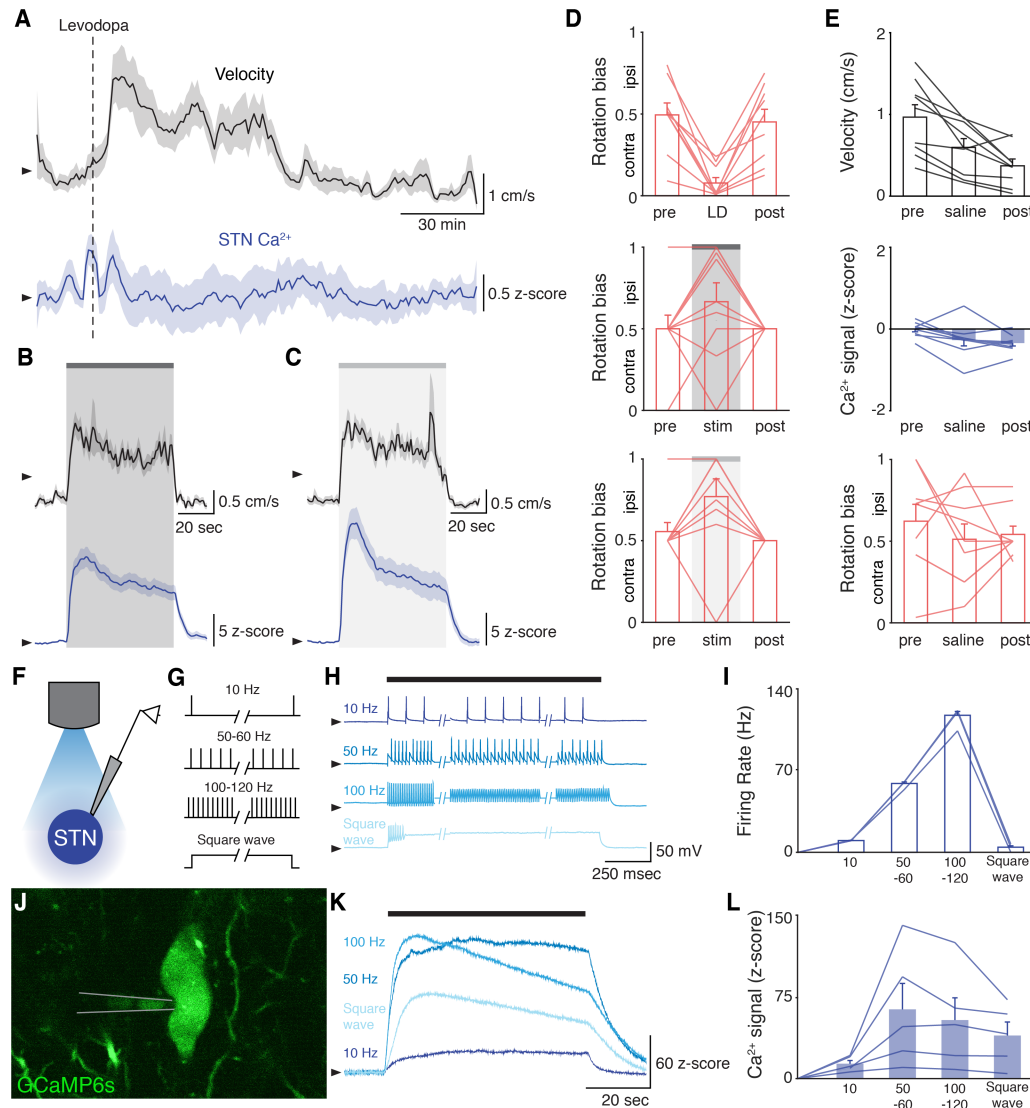
Sagittal schematic showing viral injection and optical fiber implantation in the STN. Right: Postmortem sagittal section showing ChR2 expression (inset, scale=500  $\mu$ m). (I-K) Ex vivo recordings of STN neurons in the cell-attached configuration. **(I)** Recording configuration. **(J)** Representative STN neuron before, during, and after pulsatile blue light stimulation (1 min, 50Hz). 1 second portions of the sweep are shown below. **(K)** Average firing rate before, during, and after blue light stimulation (n=13 cells, N=3 mice). **(L)** Representative single-session velocity in response to 50 Hz blue light stimulation. **(M)** Average velocity before, during, and after 50 Hz blue light stimulation (N=8 mice). **(N)** Average rotation bias of parkinsonian mice before, during, and after stimulation (N=8 mice). Arrowhead in cell-attached recordings and velocity traces corresponds to 0 pA and 1 cm/s, respectively. Bar plots show mean  $\pm$  SEM.

## Supplemental Figure 3.1



**Supplemental Figure 3.1. Related to Figure 3.1. Levodopa and STN DBS produce similar behaviors in parkinsonian mice.** Hemiparkinsonian mice were treated with levodopa (A-E) or STN DBS (F-N). **(A)** Representative single-session velocities before and after levodopa injection (dotted line) in 3 mice. **(B)** Average velocity over time, **(C)** Binned average velocity (left-middle), **(D)** rotational bias, and **(E)** dyskinesia in response to levodopa injection (N=32 mice). **(F)** Representative single-session velocities in response to 60 Hz STN DBS in 3 mice. **(G)** Average velocity over time, **(H)** binned average velocity, **(I)** rotational bias, and **(J)** dyskinesia in response to 60 Hz STN DBS (N=39 mice). **(K)** Representative single-session velocities in response to 100 Hz STN DBS in 3 mice. **(L)** Average velocity over time, **(M)** binned average velocity, **(N)** rotational bias, and **(O)** dyskinesia in response to 100 Hz STN DBS (N=36 mice). Arrowhead in velocity traces corresponds to 1 cm/s. Bar plots show mean  $\pm$  SEM.

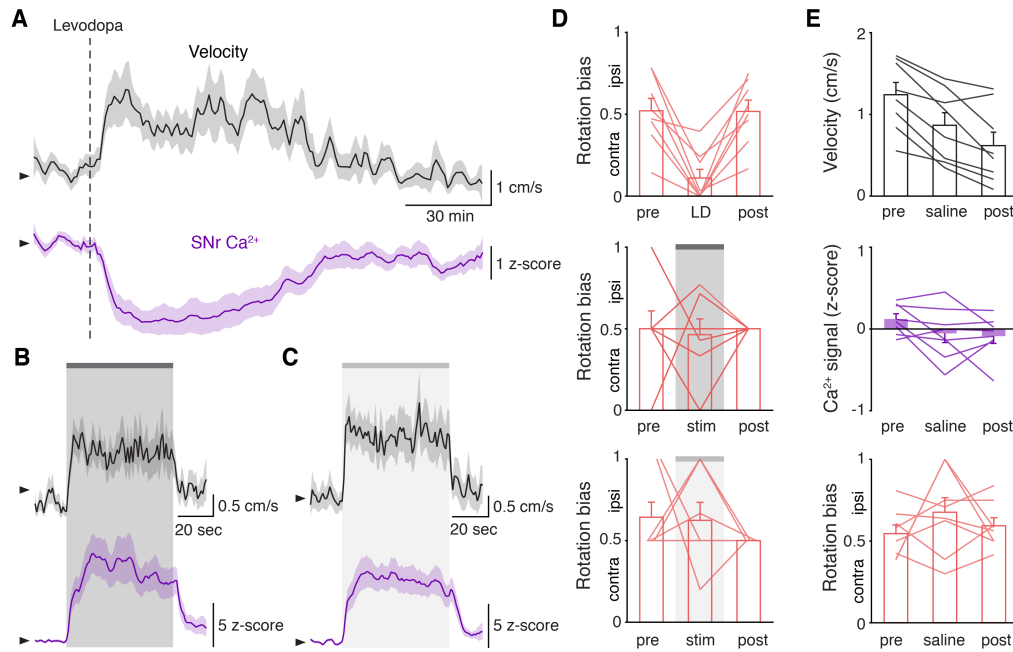
## Supplemental Figure 3.2



**Supplemental Figure 3.2. Related to Figure 3.1. STN stimulation increases STN activity in vitro and in vivo.** VGlut2-Cre mice were injected with Cre-dependent GCaMP6s in the STN. **(A-C)** Average velocity over time (black) and STN GCaMP signal (blue) following administration of levodopa (H, N=9 mice), 60 Hz STN DBS (I, N=9 mice), or 100 Hz STN DBS (J, N=9 mice). **(D)** Average rotation bias before, during, and after levodopa (top, N=9 mice), 60 Hz STN DBS (middle, N=9 mice), or 100 Hz STN DBS (bottom, N=9 mice). **(E)** Average velocity (top), STN GCaMP signal (middle), and rotational bias before, during, and after saline injection (N=9 mice). **(F-L)** Combined electrophysiological and calcium imaging recordings in STN neurons from ex vivo slices. Neurons were patched in the whole-cell current-clamp configuration. **(F)** Recording configuration. **(G)** Schematic showing current-clamp stimulation protocol. **(H)**

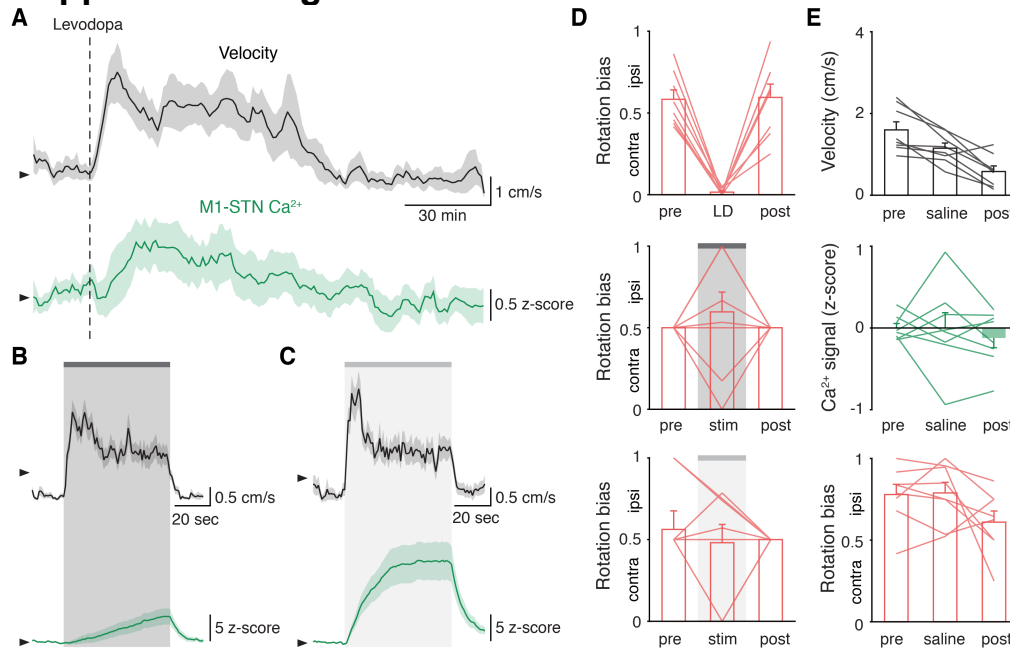
Representative STN neuron responses to the indicated current-clamp stimulation. **(I)** Average firing rate of STN neurons in response to stimulation (n=5 cells, N=2 mice). **(J)** Image of GCaMP-expressing STN neuron. **(K)** Representative trace of Z-scored STN GCaMP signal in response to current-clamp stimulation. **(L)** Average Z-scored STN GCaMP signal in response to current-clamp stimulation (n=5 cells, N=2 mice). Arrowhead in voltage-clamp traces, velocity traces, and GCaMP traces corresponds to -75 mV, 1 cm/s, and 0 z-score, respectively. Bar plots show mean  $\pm$  SEM.

### Supplemental Figure 3.3



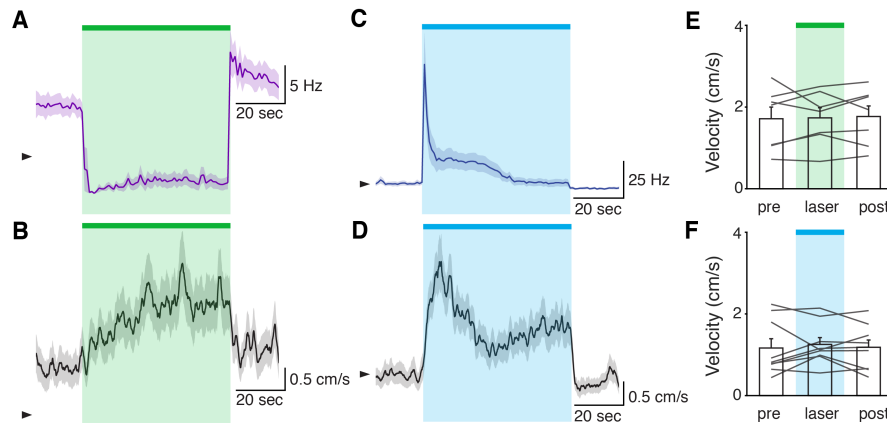
**Supplemental Figure 3.3. Related to Figure 3.2. STN DBS evokes a rapid increase in SNr activity.** Hemiparkinsonian mice were injected with GCaMP6s in the SNr and implanted with an electrical DBS device in the STN and an optical fiber in the ipsilateral SNr. **(A-C)** Average velocity over time (black) and SNr GCaMP signal (purple) following administration of levodopa (A, N=8 mice), 60 Hz STN DBS (B, N=7 mice), or 100 Hz STN DBS (C, N=7 mice). **(D)** Average rotation bias before, during, and after levodopa administration (top, N=8 mice), 60 Hz STN DBS (middle, N=7 mice), or 100 Hz STN DBS (bottom, N=7 mice). **(E)** Average velocity (top), SNr GCaMP signal (middle), and rotational bias before, during, and after saline injection (N=8 mice). Arrowhead in velocity traces and GCaMP traces corresponds to 1 cm/s and 0 z-score, respectively. Bar plots show mean  $\pm$  SEM.

### Supplemental Figure 3.4



**Supplemental Figure 3.4. Related to Figure 3.3. STN DBS drives inconsistent and slow changes to hyperdirect M1 activity.** To target hyperdirect pathway (STN-projecting M1) neurons, hemiparkinsonian mice were injected with a retrograde virus encoding Cre in the STN, and Cre-dependent GCaMP6s in the ipsilateral M1 cortex. **(A-C)** Average velocity over time (black) and M1-STN GCaMP signal (green) following administration of levodopa (A, N=8 mice), 60 Hz STN DBS (B, N=9 mice), or 100 Hz STN DBS (C, N=8 mice). **(D)** Average rotation bias before, during, and after levodopa administration (top, N=8 mice), 60 Hz STN DBS (middle, N=9 mice), or 100 Hz STN DBS (bottom, N=8 mice). **(E)** Average velocity (top), M1-STN GCaMP signal (middle), and rotational bias before, during, and after saline injection (N=8 mice). Arrowhead in velocity traces and GCaMP traces corresponds to 1 cm/s and 0 z-score, respectively. Bar plots show mean  $\pm$  SEM.

## Supplemental Figure 3.5



**Supplemental Figure 3.5. Related to Figure 3.4. The time course of optically evoked changes in ex vivo firing rate parallel those in in vivo movement velocity. (A,B,E)** Hemiparkinsonian VGAT-Cre mice were injected with eNpHR3.0 or eYFP in the ipsilesional SNr and implanted with an optical fiber over the SNr. (A) SNr neurons were patched in the cell-attached configuration in *ex vivo* brain slices. Average firing rate in response to continuous green light (n=17 cells, N=3 mice). (B) Average movement velocity in response to green light (N=10 mice). **(C,D,F)** Hemiparkinsonian VGlut2-Cre mice were injected with ChR2 or eYFP in the ipsilesional STN and implanted with an optical fiber over the STN. (C) STN neurons were patched in the cell attached configuration in *ex vivo* brain slices. Average firing rate in response to pulsatile (50 Hz) blue light stimulation (n=13 cells, N=3 mice). (D) Average movement velocity in response to pulsatile (50 Hz) blue light stimulation (N=8 mice). **(E)** Average movement velocity before, during, and after green light stimulation in mice injected with eYFP (N=7 mice). **(F)** Average movement velocity before, during, and after blue light stimulation in mice injected with eYFP (N=9 mice). Arrowhead in rate histograms and velocity traces corresponds to 5 Hz and 1 cm/s, respectively. Bar plots show mean  $\pm$  SEM.



# **Chapter 4:**

## **Conclusions**

## Conclusions

The work detailed here is a crucial step in understanding not only how DBS acts to alleviate symptoms of Parkinson's Disease, but also in providing a model for assessing the efficacy and mechanism of DBS in other neuropsychiatric disorders. In Chapter 1, we introduced STN DBS as a therapy for PD, and noted critical gaps in our current understanding of its mechanism. In Chapter 2, we established and characterized the first parkinsonian mouse model of electrical STN DBS. We used the model to characterize the relationship between stimulation parameters and therapeutic efficacy. We developed a simple composite metric for the stimulation parameters, which in turn predicted the therapeutic benefit in parkinsonian mice, in terms of movement velocity. Excitingly, this relationship was (1) linear, and (2) held even when applied retrospectively to human data. In Chapter 3, we utilized our mouse model to observe how STN DBS and levodopa alter activity in the STN and two connected regions within basal ganglia circuits, and then demonstrated that the opposing effects of these two therapies are both, paradoxically, therapeutic.

However, as with most scientific inquiries, we are still left with a number of questions. First and foremost, we do not fully understand the intriguing observation that bidirectional changes in basal ganglia activity relieve parkinsonian bradykinesia. This is in direct contradiction with the predictions of the classical rate-based model of basal ganglia activity<sup>1,2</sup>, which posits that decreases in basal ganglia activity should be prokinetic, while increases in basal ganglia activity should inhibit movement (worsening parkinsonism). As noted in the Introduction and Chapter 3, though, an increasing body of literature suggests that the rate model may not fully capture the relationship between

basal ganglia activity and movement<sup>3,4</sup>. Instead, a parallel body of literature suggests that patterning and neural synchrony may drive bradykinesia in PD. Within this literature, there are further debates between those who believe LFP oscillations at a specific frequency reflect the causal circuit mechanisms of PD, and those who suspect other elements of pattern, such as rhythmic bursting, may drive parkinsonism<sup>5-9</sup>. Disruption of either of these electrophysiological abnormalities (oscillations or rhythmic bursting) might then relieve the motor symptoms of PD. In fact, it may be that both increases or decreases in overall firing rates disrupt pathological oscillations, or that both increases and decreases in firing rates can regularize firing patterns. Though we suspect that our results may support some of these theories, we will discuss shortly the technical limitations that to date prevent us from fully addressing this question.

In considering how DBS might relieve parkinsonian motor deficits, another area for future study lies outside of the basal ganglia. While we addressed how STN DBS changes the activity of both a key STN input (hyperdirect pathway M1 neurons) and its canonical output (the SNr), the STN projects out of the basal ganglia to a number of motor-related structures, particularly the mesencephalic locomotor region (MLR). As its name suggests, the MLR has been implicated in locomotor control<sup>10-12</sup>. Even more strikingly, a subregion of the MLR, the pedunculopontine nucleus (PPN) shows changes in connectivity and activity in parkinsonian rats<sup>13</sup> and direct stimulation of the PPN may help to alleviate parkinsonian symptoms in humans<sup>14</sup>, although results have been mixed<sup>15</sup>. It will be important for future studies to explore the possible involvement of areas such as the MLR in mediating the therapeutic effects of STN DBS.

When I began investigating STN DBS, I had the rather lofty goal of unraveling the mechanism of DBS during the course of my PhD. Though I believe we have made crucial progress towards this goal, there is without a doubt more work to be done. How, then, might we conceive of a path forward? Though we were able to avoid the electrical artifacts that have hindered electrophysiological recordings during DBS in the past, our recording method did not achieve single-cell resolution, nor did it use a signal that varied on the time scale of voltage. I believe that in order to determine how STN DBS exerts its therapeutic benefit, we will need to overcome both of these limitations so that we can assess how STN DBS affects synchrony and patterning among individual neurons.

Achieving single-cell resolution is perhaps the easier of the two. Rather than using bulk fiber photometry calcium imaging, we have begun to image GCaMP in individual cells during STN DBS using a GRIN lens and a CMOS chip<sup>16</sup>. This has provided us with our first look into how individual neurons respond to stimulation, and has the potential to reveal changes bursting, or in the synchronization of calcium signals across a population of neurons. However, the current generation of calcium sensors are far too slow to reflect individual action potentials, especially in areas like the STN or SNr, where neurons fire tonically at very high rates<sup>17</sup>. Ideally, one would use genetically encoded voltage indicators<sup>18</sup> (GEVIs) rather than calcium indicators, given that they can be imaged at much higher rates *and*, perhaps even more importantly, their output directly corresponds to neuronal spiking. So far, while GEVIs have been used to perform bulk-voltage imaging<sup>19</sup> in freely behaving animals, or to perform head-fixed recordings of individual neurons in small groups<sup>20</sup>, the combination of freely moving, single-cell, high spatial resolution, and fast acquisition rate have yet to be attained, particularly in deep structures.

In large part this is a technical problem; commercial CMOS chips were never intended for the speeds and resolutions ideal for large-scale GRIN lens voltage imaging. It is likely, given the pace of technology, that we will eventually have the ability to perform these types of recordings, but until then it will be challenging to apply our optical methods to more satisfyingly identify the mechanisms underlying STN DBS.

Despite these limitations, the knowledge obtained here can still be utilized, along with other models and physiological techniques, to inform improvements in STN DBS in PD. In addition, our approach may be useful as other investigators explore other neuropsychiatric diseases for which STN DBS might prove therapeutic. Having now established a model of electrical STN DBS, we are excited to assess the efficacy of basal ganglia DBS in other movement disorders, including those which have not yet been treated with DBS. As greater knowledge of the circuit mechanisms of other neuropsychiatric diseases is developed, mouse models of DBS may also help provide a rational framework for the identification of new DBS targets or modes of stimulation. Given the wide array of disease models available in mice and the relative ease of high throughput studies, we see this as the ideal tool for screening and assessing the efficacy of STN DBS before testing in human patients.

## References

1. Albin, R. L., Young, A. B. & Penney, J. B. The functional anatomy of basal ganglia disorders. *Trends Neurosci.* **12**, 366–375 (1989).
2. DeLong, M. R. Primate models of movement disorders of basal ganglia origin. *Trends Neurosci.* **13**, 281–285 (1990).
3. McIver, E. L. *et al.* Maladaptive Downregulation of Autonomous Subthalamic Nucleus Activity following the Loss of Midbrain Dopamine Neurons. *Cell Rep.* **28**, 992-1002.e4 (2019).
4. Cui, G. *et al.* Concurrent Activation of Striatal Direct and Indirect Pathways During Action Initiation. *Nature* **494**, 238–242 (2013).
5. Little, S. & Brown, P. The functional role of beta oscillations in Parkinson's disease. *Parkinsonism Relat. Disord.* **20 Suppl 1**, S44-48 (2014).
6. de Hemptinne, C. *et al.* Therapeutic deep brain stimulation reduces cortical phase-amplitude coupling in Parkinson's disease. *Nat. Neurosci.* **18**, 779–786 (2015).
7. Swann, N. C. *et al.* Gamma Oscillations in the Hyperkinetic State Detected with Chronic Human Brain Recordings in Parkinson's Disease. *J. Neurosci.* **36**, 6445–6458 (2016).
8. Pan, M.-K. *et al.* Neuronal firing patterns outweigh circuitry oscillations in parkinsonian motor control. *J. Clin. Invest.* **126**, 4516–4526 (2016).

9. Tai, C.-H., Yang, Y.-C., Pan, M.-K., Huang, C.-S. & Kuo, C.-C. Modulation of subthalamic T-type Ca<sup>2+</sup> channels remedies locomotor deficits in a rat model of Parkinson disease. <https://www.jci.org/articles/view/46482/figure/10> (2011) doi:10.1172/JCI46482.
10. Lee, A. M. *et al.* Identification of a brainstem circuit regulating visual cortical state in parallel with locomotion. *Neuron* **83**, 455–466 (2014).
11. Roseberry, T. K. *et al.* Cell-Type-Specific Control of Brainstem Locomotor Circuits by Basal Ganglia. *Cell* **164**, 526–537 (2016).
12. Norton, A. B. W., Jo, Y. S., Clark, E. W., Taylor, C. A. & Mizumori, S. J. Y. Independent neural coding of reward and movement by pedunculo-pontine tegmental nucleus neurons in freely navigating rats. *Eur. J. Neurosci.* **33**, 1885–1896 (2011).
13. Martinez-Gonzalez, C., van Andel, J., Bolam, J. P. & Mena-Segovia, J. Divergent motor projections from the pedunculo-pontine nucleus are differentially regulated in Parkinsonism. *Brain Struct. Funct.* **219**, 1451–1462 (2014).
14. Moro, E. *et al.* Unilateral pedunculo-pontine stimulation improves falls in Parkinson's disease. *Brain* **133**, 215–224 (2010).
15. Ferraye, M. U. *et al.* Effects of pedunculo-pontine nucleus area stimulation on gait disorders in Parkinson's disease. *Brain J. Neurol.* **133**, 205–214 (2010).
16. Ghosh, K. K. *et al.* Miniaturized integration of a fluorescence microscope. *Nat. Methods* **8**, 871–878 (2011).

17. Chen, T.-W. *et al.* Ultra-sensitive fluorescent proteins for imaging neuronal activity. *Nature* **499**, 295–300 (2013).
18. Xu, Y., Zou, P. & Cohen, A. E. Voltage Imaging with Genetically Encoded Indicators. *Curr. Opin. Chem. Biol.* **39**, 1–10 (2017).
19. Marshall, J. D. *et al.* Cell-type specific optical recording of membrane voltage dynamics in freely moving mice. *Cell* **167**, 1650-1662.e15 (2016).
20. Piatkevich, K. D. *et al.* Population imaging of neural activity in awake behaving mice. *Nature* **574**, 413–417 (2019).



## Publishing Agreement

It is the policy of the University to encourage open access and broad distribution of all theses, dissertations, and manuscripts. The Graduate Division will facilitate the distribution of UCSF theses, dissertations, and manuscripts to the UCSF Library for open access and distribution. UCSF will make such theses, dissertations, and manuscripts accessible to the public and will take reasonable steps to preserve these works in perpetuity.

I hereby grant the non-exclusive, perpetual right to The Regents of the University of California to reproduce, publicly display, distribute, preserve, and publish copies of my thesis, dissertation, or manuscript in any form or media, now existing or later derived, including access online for teaching, research, and public service purposes.

DocuSigned by:

*Jonathan Schor*

FAEF6CB22D0A4EE...

Author Signature

6/9/2020

Date